Physics – Uspekhi **43** (6) 541 – 572 (2000)

REVIEWS OF TOPICAL PROBLEMS

PACS numbers: 61.16.Ch, 62.20. Qp, 68.35.Gy, **73.20. – r**, 81.40.Pq

Nanotribology: experimental facts and theoretical models

G V Dedkov

DOI: 10.1070/PU2000v043n06ABEH00650

Contents

Abstract. Nanotribology is a new physical discipline in which friction, adhesion, wear and lubrication are studied within a unified framework at the nanoscopic level. In this paper, the experimental and theoretical problems of topical interest in this field are reviewed. In the analysis of the experimental data, emphasis is placed on 'dry' adhesive friction between the probe of a scanning frictional microscope and an atomically smooth surface. On the theoretical side, studies related to the mechanisms of adhesive (static) and dynamic (velocity proportional) friction are discussed and results on the electromagnetic, electron, and phonon effects as well as molecular dynamics results are presented. Studies using the method of quartz crystalline microbalance and the 'surface force' concept are briefly reviewed.

1. Introduction

The study of the nature of friction forces on the atomic level was made possible with the advent of the atomic force microscope [1, 2]. In a decade, rapid progress in this fundamentally new method of physical investigation lead to the establishment of vast new field of physics — nanotribology — which combines experimental and theoretical studies of adhesion, friction, wear and lubrication, chemical activity and triboelectromagnetism on the nanostructural level [3 – 11].

Only recently, problems associated with friction were for the most part of an engineering character and might be thought of as 'dirty' physics, since the macroscopic contacts of surfaces in the literal sense are dirtied by absorbed particles, wear products and lubricants. However, as was often the case in science history, what only yesterday seemed to be archaic, today takes on a new meaning — and now one can say without exaggeration that the old science dealing with friction (tribology), the foundations of which were laid down by Amonton three hundred years ago, has received a second birth.

An understanding of the key role of numerous individual microcontacts appearing between contacting surfaces has given impetus to the development of nanotribology. The total area of such contacts (the area of actual contact) can be much less than the apparent area [6, 12].

With the transition to a qualitatively new level of investigation, it turned out that physical processes in tribocontacts are considerably more intricate and diverse than had been suspected and include a wealth of new phenomena such as phase transitions resulting from the shear ordering of thin films in the 'probe-surface' contact and the formation of contact 'bridges' [4], chemical, electrochemical and triboelectrical effects [13 – 15]; effects associated with humidity [16, 17], superconductivity [18] and so on.

Along with atomic force microscopy (AFM) and friction microscopy, experiments carried out with the use of surface force apparatus [4, 19, 20] and the quartz crystal microbalance technique [21 – 23] occupy an important place in the studies of nanotriboeffects. These experimental methods presently hold the greatest promise for nanotribology. The

G V Dedkov Kabardino-Balkarian State University,
360004 Nal'chik, Russian Federation
Fax (7-095) 337-99 55
E-mail: gv_dedkov@rekt.kbsu.ru

Received 17 July 1999, revised 5 March 2000
Uspekhi Fizicheskikh Nauk **170** (6) 585 – 618 (2000)
Translated by V M Matveev; edited by S D Danilov

rapidly progressing surface nanoindentation technique may be also assigned to these methods.

Scanning tunnelling microscopy (STM) developed before AFM [25] organically combines with the latter, since most present-day probing microscopes operate in the multimode regime including both STM and AFM modes.

The study of friction and processes associated with it on the nanostructural level is of great interest for a broad spectrum of technical applications such as the technology of production and surface coating of hard magnetic disks for computers, the fabrication of microsensors and so on. These and the traditionally important engineering applications of tribology in machine construction require a deeper insight into the properties of materials on the atomic level with the aim of optimizing and forecasting the tribological characteristics of friction surfaces. Successful solution of these problems calls for decreasing the existing gap between the macro- and nanostructural levels of knowledge of the properties of material in general and friction in particular.

Unfortunately, experimental information in the field of nanoprobing microscopy and tribology has accumulated so rapidly that the theoretical description of many effects still remains unsatisfactory, even though a number of important recent results were successfully predicted and/or interpreted using the molecular dynamics (MD) method and classical contact mechanics. Although 'dry' friction does not depend on the visible area of a contact and practically does not depend on the slip velocity, its seeming simplicity is deceptive, since it is determined by a complex diversity of properties of surfaces, by the presence of numerous microcontacts, effects of an adhesive and deformative nature as well as 'ploughing' of the surface with microroughness and wear products.

There exist several levels of complexity in the effort to understand the nature of adhesive friction — the most intricate and least known mechanism. One of these levels is associated with the necessity of developing a detailed atomic theory of triboprocesses describing adhesion, friction and wear using an unified approach within the framework of the atomic models of chemical bonding and elementary electron – phonon processes responsible for energy dissipation.

Another level concerns the slip mechanism. For the present we are not in a position to state whether the relative movement of contacting surfaces is continuous or a series of discrete events of sticking and slipping. If the second scenario is realized, what are the values of the displacement and time interval corresponding to an elementary microslip? Many experimental works point to the fact that the stick-slip effect exhibits lattice periodicity [3] enabling one to obtain the atomic contrast of a surface in the lateral AFM mode. However, it is possible only in the case of atomically smooth surfaces, whereas most often the contact area is contaminated by adsorbed substances and wear products. These causes result in the existence of a gap between experimental and theoretical nanotribology. There also exist some problems of an instrumental nature which do not always allow one to make an adequate correlation of theoretical models with experiment (for example, the problems of calibration of experimental results).

The main aim of this paper is to make a critical analysis of the experimental and theoretical results obtained in this new field over the last five or six years, although some of the problems concerned have been elucidated to a greater or lesser extent of completeness by a number of foreign authors [3, 11, 26]. At the same time, an attempt is made to construct some integral physical picture specific to nanotribocontacts — the elementary areas of friction. Many results presented in this paper have not yet been discussed in the literature, and efforts to systematize theoretical notions are of a fragmentary character, since the basic calculation models are still under development and there is no commonly accepted point of view on some of these models. This concerns problems relating to the interpretation of the stick-slip effect, adhesive friction models, the dynamical mechanisms of noncontact friction and so on.

On the whole, in deciding on the problems to be discussed in this review, both its restricted volume and the subjective viewpoint of the author have undeniably contributed. Therefore, in particular, when discussing theoretical models, much attention is given to the problem of 'dry' adhesive friction and noncontact (dynamical) friction in vacuum. An understanding of these elementary processes brings us nearer to an understanding of the nature of friction as a whole. The 'ploughing' effect, 'wet' friction, the thermodynamical aspects of the problem and a diversity of other questions call for special consideration. Some of these questions are partially discussed in works [25 – 30]. It should also be noted that, though the main line of development of nanotribology is associated with the application of probing microscopy, the discussion of the methods and results of the latter is not the subject of the review and is presented only in connection with the consideration of tribology problems.

The review has the following structure. Section 2 is a brief review of the basic modes of operation of the AFM and other methods used in experimental investigations of micro- and nanocontacts. In Section 3, on the basis of the available experimental data, some physical processes in tribocontacts such as the stick-slip effect, adhesion, chemical and other effects are discussed. The existing theoretical notions providing an interpretation of experimental data are considered in parallel. On the whole, this part of the review is of a descriptive character, and it ends with the formulation of some important experimental problems facing specialists in the field of tribology.

Section 4 is entirely devoted to theoretical models. It begins with the discussion of the contact-mechanics approximations and their use for interpretation of AFM data on 'dry' adhesive friction in vacuum. Then the simple models of the lateral movement of a probe providing an interpretation of the experimental images of a surface are considered, and the evolution of the structure of nanocontacts observed with the use of the molecular-dynamics method is discussed in detail. Furthermore, the mechanisms of static (velocity-independent) and dynamic (velocity-proportional) friction are considered, the application of theoretical models to the explanation of the experimental dependences 'friction force – loading force', the stick-slip effect, the effect of damping the adsorbed-film movement in quartz crystal microbalance experiments and so on is analyzed. Other theories, for example, the theory of rubber friction with a stiff surface are discussed more briefly.

Section 5 is concerned with applications of the results of nanotribological investigations in present-day technologies. The 'probe – surface' interaction allows one not only to determine the structure of the contact area on an atomic scale, but also to modify the properties of a surface. In particular, the portions of the tunnelling contact of a probe with a passivated silicon surface undergo selective oxidation. This makes it possible to perform nanolithography directly in

the mode of contact scanning. To reduce processing time, it is necessary to increase the scanning speed up to 1 cm s^{-1}. There is no question that the achievements of scanning probing microscopy, nanotribology and nanotechnology are capable of leading to a revolution in microelectronics in the near future.

2. Basic modes of operation of atomic force microscopes

Following pioneer works by Binnig et al. [1] as well as Mate et al. [2], the AFM technique has gained leading positions in studies of nanostructural friction. Forces acting between a sharp probe (tip) placed in close contact with a sample and the surface of the latter result in a measurable deformation of a cantilever (console) to which the probe is attached. Fig. 1a illustrates a widely used mode of operating the AFM on the basis of optical detection of the probe position. Other methods are described, for example, in works [30, 31] (see also references in Ref. [3]).

The cantilever bends in the vertical direction upwards or downwards because of a repulsive or attractive interaction, and the value of its deformation is directly proportional to the value of the counterpoising elastic force. The lateral forces result in torsion deformation relative to an equilibrium position. When the system is at equilibrium, the forces, which are responsible for bending and twisting, are balanced out by the elastic forces of the cantilever. These latter are modelled by equivalent springs with 'normal' and 'lateral' stiffness.

It should be noted that the lateral forces can be determined not only by friction, but also by the local slope of the surface [3, 32]. Besides, there always exists some relation between the normal force and the lateral force, especially in the case when the latter is directed along the axis aligned with the long side of a cantilever.

One further reason can be that the probe is positioned at a small angle α to the horizontal to ensure contact with the surface rather than the plane side of the cantilever. Since the probe has a height of the order of several microns, the microroughness of such a scale may catch on the cantilever [33]. As a result of this slope of the probe, its normal and lateral displacements are related by the following equation: $\Delta z = \Delta x \cot \alpha$.

Quantitative analysis of the lateral and normal forces in the AFM requires knowledge of the normal and lateral stiffness of the cantilever, on the one hand, and the geometry of the probe, on the other. Calculation formulas for the stiffness with regard to different geometries of cantilevers can be found, for example, in Ref. [34]. Recently, a direct method for determination of the lateral stiffness *in situ* was proposed. For a cantilever in the form of a rectangular parallelepiped, the normal and lateral elastic stiffness are [35]

$$k_n = \frac{Ebt^3}{4a^3}, \tag{2.1}$$

$$k_l = \frac{Gbt^3}{3aH^2}, \tag{2.2}$$

where E and G are Young's modulus and the shear modulus, respectively, b and t are the linear dimensions of the cross section of the cantilever, a is the length of the cantilever measured from the point of its clamping to the point of attachment of the probe, H is the length of the probe (tip) of the AFM measured from the neutral (long) axis of the console to the apex point of the probe. For commercial silicon cantilevers, typical values of constants (2.1) and (2.2) are of the order of 1 and 100 m^{-1}, respectively.

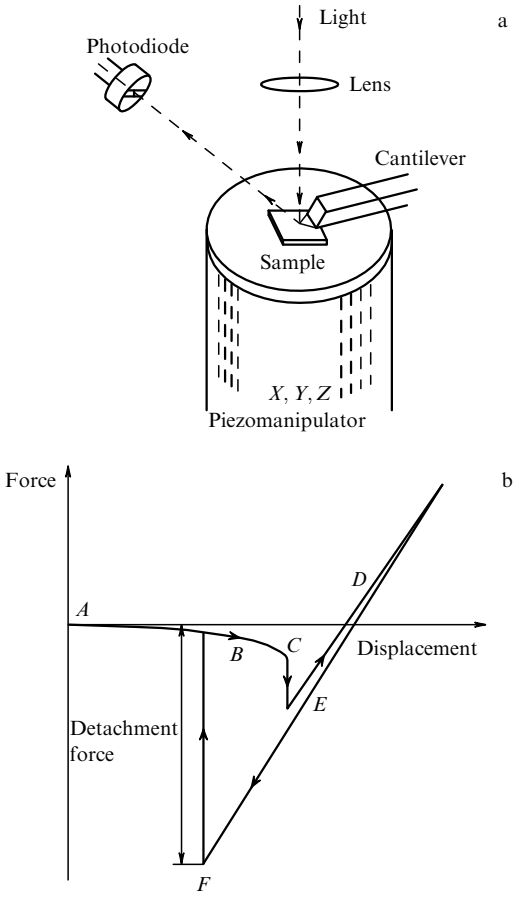

Figure 1. (a) Scheme of an AFM with optical detection of the cantilever displacement. The sample is moved by a piezomotor having three degrees of freedom (X, Y, Z). The displacements corresponding to the surface topography are used for the formation of an image. (b) Force curve of the lowering/lift of a probe to/from a surface shows the dependence of the force applied to a contact (vertical bending of the cantilever) on the distance between the cantilever and sample: on portion A of the curve there are no probe–surface forces, since the probe is far from the surface; B — a stable attractive regime under the action of the Van-der-Waals forces; C — the gradient of the attractive force exceeds the normal stiffness of the cantilever, therefore the probe loses stability and suddenly 'sticks' to the surface; D — further decreasing the distance between the probe and the sample; E — the movement of the cantilever is reversed in order to avoid probe disruption; adhesion between the probe and the surface holds the contact under the action of a stretching force; F — the stretching force exceeds the critical force of detachment, and the probe 'falls off' the surface.

Another practically important formula determines the fundamental resonance frequency for the vertical oscillation of a cantilever:

$$\Omega_0 = \frac{1.95b}{a^2}\sqrt{\frac{E}{3\rho}}, \tag{2.3}$$

where ρ is the density of the console material. The resonance frequency of lateral oscillation (corresponding to bending deformations) is obtained by multiplying expression (2.3) by b/t. Using formulas (2.1)–(2.3), one can define an 'effective' mass of an equivalent oscillator by the formula $k = m_{\text{eff}}\Omega_0^2$.

Generally, with allowance for the linkage of the probe with the surface, the determination of the resonance frequency is a rather complicated task, and the point-mass approximation used to describe the oscillatory motion dynamics may result in a considerable error. Despite this fact, the simple harmonic model is widely used for the description of the modulation mode of the AFM.

2.1 Normal force measurement mode

Figure 1b shows schematically the 'force – displacement' curve reflecting the dependence of the vertical bending of a cantilever and the force applied to a contact on the vertical distance between the sample and the remote (not deformed) part of the cantilever [3]. The different portions of this curve correspond to the following situations: A — the absence of any interaction force; B — the first stage of attraction to the surface; C — the 'sticking' of the probe to the surface occurring at the instant when the gradient of an attractive force acting from the surface exceeds the normal stiffness of the cantilever; D — the contact (repulsive) mode; since the probe operates in the mode of repulsive interaction with the surface, the cantilever is concave towards the surface, and the force loading the contact is positive and corresponds to the external force; E — the movement of the console is reversed in order to avoid probe disruption; owing to adhesive forces, contact is not lost when the applied force changes its sign and becomes negative; now the cantilever is concave upward; F — a negative force applied to the cantilever and tending to detach the probe from the surface exceeds the critical force of adhesive sticking, and the probe 'falls off' the surface.

Figure 1b allows one to distinguish two main modes of interaction of the probe with the sample: the attractive mode (determined by Van-der-Waals, capillary, electrostatic, magnetic forces) and the contact mode corresponding to repulsive forces. Such a classification, however, is not exactly correct, since different parts of the probe can simultaneously undergo the action of repulsive and attractive forces from surface atoms. Therefore, it is more pertinent to speak of a dominant type of interaction for the probe as a whole.

In the first experiments the AFM was used for measuring the surface topography. In such experiments a feedback loop was used to maintain the vertical displacement of the cantilever or the normal force at a constant value when scanning along the surface. The corresponding 'constant-height' and 'constant normal force' modes allow one to obtain atomic resolution both in the repulsive and attractive modes. Figure 2 illustrates the indicated modes as well as so-called 'error-signal' and 'modulation' modes.

In the constant-height mode, the feedback loop maintains the distance between the apex of the probe and the surface at a constant value. The feedback signal is calibrated as the probe height above the surface. However, the residual (not compensated) displacement of the cantilever exists, since otherwise the feedback loop does not operate. This signal is used in the error-signal mode.

In the case of mechanical contact of the probe with the surface the contact area includes many atoms, therefore the contact mode of the AFM does not generally provide atomic resolution of a surface.

2.2 Lateral force measurement mode

The lateral twisting of a cantilever can be detected simultaneously with the surface topography. The peculiarities of a surface profile which are not resolved in other modes can be visualized owing to the distinctions of friction characteristics of the surface.

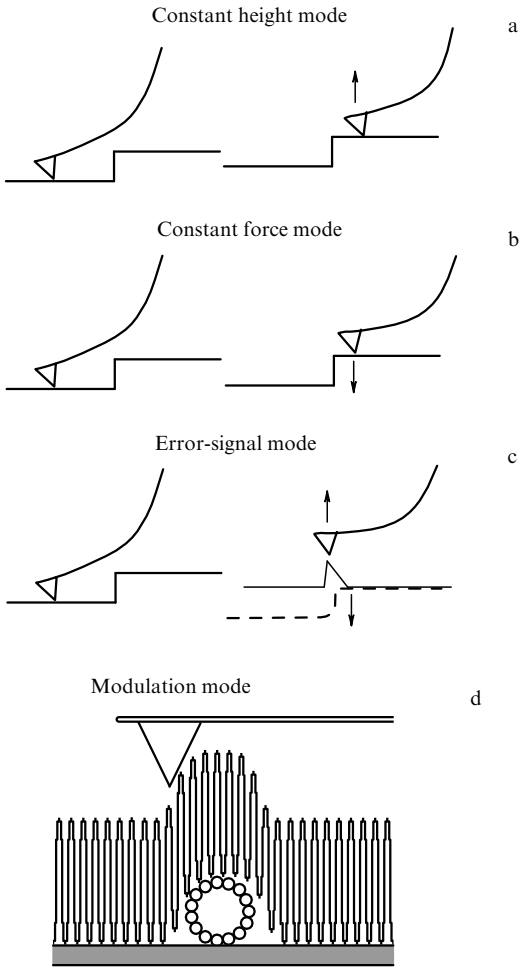

Figure 2. Basic operating modes of AFMs. The arrows show the movement of the cantilever and the sample. (a) In the constant-height mode, the sample moves horizontally and the displacements of the cantilever are monitored. The synchronous (with scanning) recording of the height is the topographic (force) image of a surface. (b) In the constant-force mode, a feedback loop prevents large displacements of the probe down to and up from the surface. The variations of the displacements of the cantilever are minimized owing to the adjustment of coordinate z by the feedback loop so that the deformation of the cantilever remains constant. The feedback signal is calibrated as the probe height above the surface. (c) In the error-signal mode, the residual (not compensated by the feedback loop) movement of the cantilever is used. (d) In the modulation mode, the cantilever oscillates in the vertical direction under the action of a periodic force. The amplitude of oscillation is monitored synchronously with the displacement of the probe in the (x, y) plane. One can also monitor the variations of frequency or phase of cantilever vibration. By analogy with the normal-contrast mode, one can use the lateral-contrast mode. In the latter case the modulation mode is also possible.

Surface images in the lateral force mode reflect the stick-slip (SS) effect exhibiting a periodicity of the lattice constant corresponding to a given sample [39, 40]. An understanding of the physics of this effect still remains unsatisfactory, since the contact area generally involves a large number of atoms (10 – 10000). It is unclear how such a large group of atoms transfers over the interatomic distance as a whole. When measuring the lateral forces on alkaline-haloid crystals, a periodicity corresponding to one-half the lattice constant is also observed [3, 39].

In these experiments such an important characteristic as the 'friction force – loading force' dependence is measured [35, 41 – 43]. It is obtained by subtraction of the average values of a lateral force applied to the cantilever in the process of scanning the surface in the direct and reverse directions. The normal force is maintained constant, and the difference of the average values of the lateral force is taken with a factor of 1/2. A 'friction loop' obtained in the process of the probe movement is shown in Fig. 3 [43]. Periodical spikes of the lateral force are related to the SS effect. After passing one loop, the value of the normal force changes and the process repeats. Thus, a series of the average values of friction forces is determined corresponding to given loads. One disadvantage of this method is that with decreasing the load the probe is forced out of contact predominantly in the regions of lesser adhesion, therefore the portions of the surface with higher adhesion do not exhibit friction at the least applied loads.

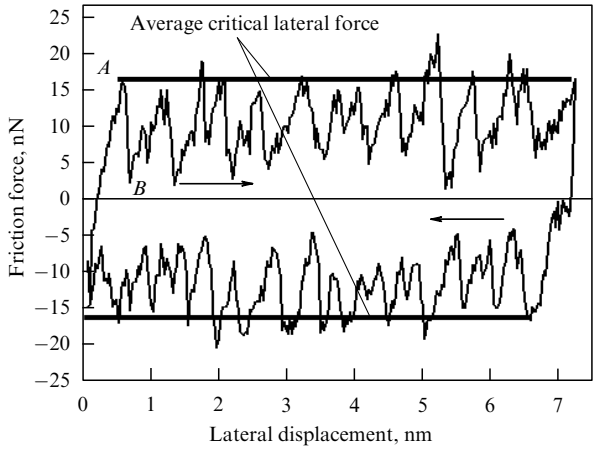

Figure 3. 'Friction loop' of lateral forces corresponding to the stick-slip mode measured by scanning a silicon nitride probe over the KF(001) surface in vacuum. The arrows point in the direction of scanning. Hysteresis suggests the presence of energy dissipation. The average and maximum values of lateral forces for each scanning direction are indicated. (Reproduced with the permission of Salmeron [39], copyright of the American Physical Society, 1998.)

We will revert to the detailed theoretical analysis of Fig. 3 in Section 3.1. At this point, we call attention to such interesting details as a shift of the positions of the maxima and minima of the lateral force at the direct and reverse movement of the probe as well as the fine structure of periodical spikes of the lateral force. The amplitude of variations corresponding to the fine structure is (in the case of Fig. 3) about 0.1 nN. This gives an estimation of the value of the lateral force contrast achieved in experiment. If the lateral stiffness of a tribocontact has a value of the order of 1 N m^{-1}, the equivalent spatial resolution is about 0.1 nm. Lateral resolution of the same order is typical for all basic modes of AFMs and STMs, whereas for the normal contrast the value of spatial resolution is one or two orders higher. Therefore, at the same value of the normal stiffness it is possible to measure normal forces of about 1 pN (see Section 3.2).

2.3 Modulation mode

The general idea consists in the application of an oscillating force to the probe setting it into forced vibration along the normal to the surface of a sample. Further recording the amplitude of oscillation is performed synchronously with the displacement of the probe in the horizontal plane. If a feedback loop maintains this amplitude constant, the probe 'feels' the surface (Fig. 2d). In this case one can determine the relief of a surface with atomic resolution analogous to resolution which can be obtained with the use of the normal mode.

If the probe and sample are rigid, the displacement of the latter along the normal causes mainly an elastic response of the cantilever, but if a surface is soft, it undergoes an additional compression and the response of the cantilever is decreased. Therefore, in the process of scanning at a constant height, the variations of the amplitude of probe vibration reflect local variations of the contrast of the elastic properties of the surface. Among the modifications of this method are the tapping mode [36], the extended-contact mode and the measurement of 'force – normal displacement' dependences at each point of a scan line (force surface cartography [44]). The latter mode is similar to the method used in nanoindentors, and it is considered in detail in the following section. Other versions of the modulation mode are described, for example, in paper [45].

If a cantilever is to be sensitive to the elastic properties of a sample, its stiffness must be comparable with that of the surface, since taken together they are similar to a pair of springs joined in tandem (Fig. 4a). Therefore, if one of the springs has smaller stiffness, it takes upon itself the main deformation. This constrains the sphere of application of this method to the case of relatively soft surfaces (polymers and biological tissues) if low-stiffness cantilevers are used. On the whole, this method visualizes the relative distribution of the elastic properties of the sample, since the actual area of the contact remains undetermined. The determination of the absolute values of local elastic moduli becomes possible, if the contact-mechanics approximations are used in addition for the estimation of the area of the contact.

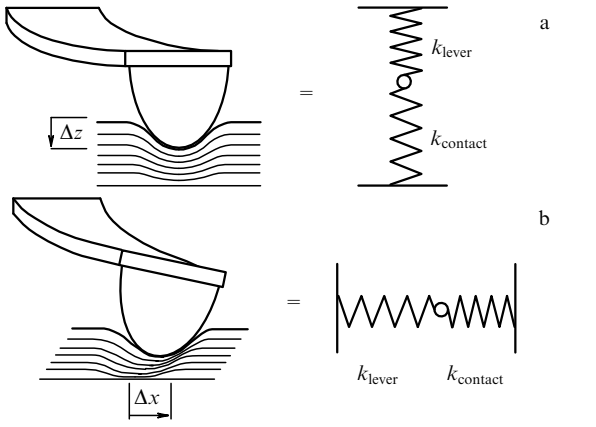

Figure 4. Normal and lateral stiffness in the AFM. The cantilever and surface undergo normal (a) and lateral (b) compression with the resulting displacements Δz and Δx, respectively. In both cases the cantilever and surface taken together are similar to a pair of springs joined in tandem. If one of the springs has smaller stiffness, it takes upon itself the main deformation. Since in experiments the total displacement of a cantilever is measured, its stiffness must be comparable with the stiffness of the contact in order that the cantilever be sensitive to the elastic properties of the sample. (Reproduced with the permission of Salmeron [39], copyright of the American Physical Society, 1998.)

2.4 Normal stiffness measurement and nanoindentors

The determination of the normal stiffness of an elastic contact is based on the relationships of contact mechanics relating the value of an applied normal force P with the deformation of the sample surface x and with the radius of the contact area a. The normal contact stiffness and the microhardness of a surface are defined as $k_c = dP/dx$ and $H = P_{max}/\pi a^2$, respectively, where P_{max} is the maximum loading force producing an impression in a sample with area πa^2 (after removing the load). These relationships form the basis of the surface indentation (microdeformation) method [46].

The original development of the indentation methods was connected with studies of the mechanical properties of materials and was not directly related to problems of nanotribology. However, progress in the development of the AFM technique has led to the 'intersection' of the corresponding methods, since an AFM probe is essentially a nanoindentor. To obtain the loading force characteristics of a contact, all one needs to do is to control the value of the normal force. The high resolution achieved with the use of the AFM allows one to investigate microhardness and many other characteristics of film coatings and microparticles with an accuracy and resolution much superior to the accuracy of standard microindentors. Nevertheless, the commercial systems of indentation on the basis of the three-cornered diamond Berkovitch indentors have now been developed to a high degree of perfection [46], and some of them provide normal force and deformation resolution not worse than 10 nN and 0.1 nm, respectively.

By applying an additional oscillating load to an indentor, one can conduct continuous measurement of the contact stiffness through monitoring the amplitudes of displacement oscillation caused by the corresponding force or through the detection of phase shifts between force and displacement oscillation. In such a manner one can also measure the viscoelastic characteristics of a contact [46].

2.5 Lateral stiffness and friction force

In a similar manner one can conduct the measurement of the lateral stiffness of a contact (Fig. 4b). For commercial AFM, this mode was first implemented in works [35, 47, 48]. The derivative of the lateral force with respect to the lateral coordinate corresponds to an equivalent stiffness of the cantilever-surface system:

$$k_e = \frac{dF}{dx} = \frac{k_l k_c}{k_l + k_c} ,$$

where k_l and k_c are the lateral stiffnesses of the cantilever and the contact, respectively. The authors of work [47] also introduce an additional stiffness determined by the elasticity of the probing tip. The resulting torsion response of the cantilever ΔF to an oscillating lateral displacement Δx is measured with the use of a synchronous detector.

With a knowledge of k_l, one can obviously find the contact stiffness k_c and then the area of the contact πa^2 using the contact-mechanics formula

$$k_c = 8a\left(\frac{2-\eta_1}{G_1} + \frac{2-\eta_2}{G_2}\right)^{-1} , \qquad (2.4)$$

where $G_{1,2}$ are the shear moduli of the probe and the sample, $\eta_{1,2}$ are the Poisson coefficients. Since typical cantilevers used in AFMs have relatively high lateral stiffnesses, the contact lateral stiffnesses can be measured for a broad spectrum of soft and hard materials [3].

In accordance with the theory developed by Bowden and Tabor [12], in the case of a 'dry' contact the friction force for an individual microcontact is determined by the following formula:

$$F = A_1\sigma_0 + \pi a^2\tau , \qquad (2.5)$$

where A_1 is the cross sectional area of a cut occurring in the process of 'ploughing' of a sample by a probe, σ_0 is the limit of yield of the surface material at lateral compression, πa^2 is the actual area of the contact, and τ is the shearing stress. In the macroscopic case, there exist an interrelation between the shear modulus and the shearing stress: $G \approx 29\tau$

By definition resulting from Amonton's law, the classical friction coefficient is equal to

$$\mu = \frac{F}{P} , \qquad (2.6)$$

where P is the normal loading force. Taking into account expressions (2.5) and (2.6), the friction coefficient can be presented in the form of a sum of two components, one of which is related to abrasive friction and the other one is related to adhesive friction: $\mu = \mu_A + \mu_{AD}$. For nanotribology, of the greatest interest are the adhesion components of the force and the friction coefficient which, as is shown in Fig. 3, allow one to 'visualize' the atomic structure of a surface. As follows from experiments carried out with the use of AFMs, formula (2.5) can be used in this case only for the determination of the average values of the friction force in the contact of a probe with a surface. Nevertheless, it holds its validity for the interpretation of experimental data in the case of elastic contacts and allows one to relate the macro- and microscopic characteristics of a surface.

2.6 Force calibration and determination of the probe shape

The geometry of the contact area is indefinite if the shape and dimensions of the probe used are unknown. It is also very difficult to determine the chemical composition of a probe in the vicinity of its apex. The indicated factors, however, are decisive, since we are trying to understand the properties of a sample that is one of two parts of the contact interface area. To obtain a surface image, commercial cantilevers with a radius of curvature (in the lower part of the probe) of the order of 10 – 50 nm are used in AFMs. In this case the atomic-scale resolution is determined by a small group of probe atoms (or adsorbed foreign particles) near its apex. Obviously it is very difficult to control this group of atoms in the process of experiment. The resolution of topographical details of a large scale is obtained as the result of convolution of the geometrical shape of the probe and a portion of the surface relief and is not always unambiguous either.

Usually, the AFM probes (tips) are characterized by the so-called aspect ratio — the ratio of their length to the radius of curvature in the lower part. The length is measured from the point where the probe diameter is equal to the quadruple radius of curvature near the apex. In the case when the aspect ratio of a relief detail is higher than that of a probe, artifacts arise resulting from the fact that the probe represents its own portrayal, since in the process of the scanning of a ridge of a surface it can only 'feel' the top part of the ridge.

If test-relief features are known or a force calibration has been performed, it is possible to determine the probe shape

in situ on a nanometer or micrometer scale [42, 49]. The *ex situ* calibration of the probe shape using transmission electron microscopy also has a wide application [35]. The authors of work [50] proposed a method for determination of the probe shape using the measurement of the backward scattering yield for a low-intensity ion beam. This can be performed in the work chamber that contains the sample.

In the process of measurements of the probe geometry, double and some other undesirable structures were revealed. Their study is crucial for obtaining AFM images, accurate measurements of forces as well as nanotribological experiments.

In connection with these problems, new possibilities were opened up owing to application of fullerenes and isolated nanowires as probing elements of AFMs. These objects have well-defined structures and high strength. So, the authors of work [51] were able to fix a single molecule of C_{60} onto the tip of an AFM, and in work [52] this was done with a nanowire. The possibility of obtaining atomic resolution with such structures was theoretically substantiated in work [53].

In contrast to rigid silicon (or silicon nitride) probes, nanowires do not fail when they make contact with a surface and restore their form after removing the load. A very important advantage of the 'nanowire – surface' contacts is the constancy of the area of the contact zone directly related to the value of the friction force. In this case we have a good chance of studying the mechanism of adhesive friction in more detail, since the area of the contact can be controlled.

For experimental nanotribology, a number of other factors are of importance. Among these are the nonlinear properties of piezoceramics, hysteresis, material creep, thermal drift and so on. An extended discussion of these questions can be found in paper [32] (see also references in Ref. [3]).

2.7 Other experimental methods

***Surface force apparatus* (*SFA*)**. The construction of this apparatus was developed by Israelachvili's group [4, 20, 26]. The device consists of two atomically-smooth plates (usually made from mica), attached to the base surface of cylinders being brought into close contact. The surfaces of the plates can be treated and/or coated by a layer of material under study in a liquid or solid state as well as can be immersed in a liquid medium under well controlled conditions. Force drivers connected to cylinder holders provide controlled normal and lateral forces to be applied to the plates as well as the maintenance of a gap between the plates with an atomic accuracy. The area of the contact and the distance are measured by optical or capacitance methods. Interatomic forces acting between the surfaces, which interact via an interlayer, can be attractive, repulsive, oscillating or can have a more complex form [4, 26].

A weakness of this method is that the lateral resolution is limited. A typical value is several micrometers. Providing vacuum conditions is also a problem. Moreover, to obtain meaningful quantitative results, in deciding on a particular material for the plates, one restricts oneself mainly to mica.

The SFA allows one to study the molecular properties of liquids and so it is especially useful for investigation of the compression properties of liquid lubricating materials. Such experiments are of great importance for the elucidation of the nature of the lateral slip. With the use of this method, the effect of exfoliation of liquid separating the plates was found when changing the distance between the plates by a value of an atom diameter [54]. In this case, periodical attractive and repulsive forces correlating with the layered (atomic) structure of the liquid interlayer were detected. This effect was also observed with the use of an AFM for the contacts of a silicon probe with the mica (graphite) surface (dodecanol was used as a liquid interlayer) [55]. Experiments carried out with the use of the SFA reveal a variety of dynamical properties and phase transitions induced by the shear ordering of a film structure separating the plates. We will return to a more detailed discussion of these effects in Section 3.4.

***Quartz crystal microbalance* (*QCM*) *method*.** This method was first used to control the growth of submonolayer films. It is realized through the measurement of a resonance frequency shift for a quartz oscillator whose resonance frequency depends on the mass of a film adsorbed on a plate. Such experiments were usually carried out to control the growth of metallic films. However, as was elucidated later, an interesting feature occurs in relation to inert gas (argon, krypton) films adsorbed on these metallic films and weakly bound with their surface. In this case the Q-factor shift for a quartz oscillator induced by the existence of friction forces between an adsorbed film and a substrate was observed [21]. This allowed one to estimate the characteristic decay time of the adsorbed film motion relative to the substrate. If the corresponding friction force acting on the adsorbate atom is proportional to the slip velocity and equal to $F = -\alpha V$, then the slip time is equal to M/α, where M is the mass of the atom. As follows from experiments, the slip time is several nanoseconds. This allows one to estimate the characteristic value of the friction force. For krypton atoms, it is about 10^{-16} nN.

Using this method, the phase transformations of adsorbed films resulting in the shifts of the resonance frequency and Q-factor of a quartz oscillator because of the transition of a film from a liquid state to a solid one were found as well [23]. The theoretical interpretation of this effect is based on the assumption that the hardened film forms an incommensurate structure with a substrate and therefore slips much further (with less friction).

In conclusion of this section, it should be noted that even the above brief discussion of experimental techniques used in present-day nanotribological investigations demonstrates a surprising variety of physical phenomena occurring on the nanostructural level. As evidenced by the foregoing, progress in their study is possible with the use of different methods that complement each other. Common to all these methods is the real possibility to measure ultra-small forces and distances visualizing the discreteness of atomic structures and interatomic interactions.

3. Physical processes in nanotribocontacts

When discussing physical processes in nanotribocontacts, we attempt not only to embrace different phenomena observed experimentally, but also, where possible, to include their theoretical interpretation. An extended consideration of some of the existing theoretical models is given in Section 4.

3.1 Stick – slip effect

The stick – slip effect is crucial for the contact mode of AFMs. On the atomic level, this effect was first observed in work [2] when measuring lateral forces which act on a tungsten probe slipping over the surface of high-oriented pyrolitic graphite.

Similar measurements were later conducted in many works (see, for example, Refs [56 – 58]) with a broad spectrum of contacting materials ranging from soft materials (silicon nitride probe — stearine acid) to hard ones (diamond – diamond) (see references in paper [3]). The surfaces of alkaline-haloid crystals (NaF, NaCl, KF, KCl, KBr) were also studied [39].

Fujisawa et al. [59] carried out a comparative investigation of the SS effect for the different combinations of probe and sample materials. The periodicity of the probe slip over a surface observed in these experiments corresponded the atomic-relief topography of the surface in the normal AFM mode, but the positions of the maxima and minima of lateral and normal forces were slightly shifted relative to each other.

No experiments are presently available in which lateral resolution would be observed without the SS effect, however, a frequently observed lateral contrast is even higher than the corresponding normal contrast. Because of this the authors of works [33, 73] believe that the periodicity of lateral interaction is responsible for the overall contrast observed including normal-mode topographic images.

The SS effect was also observed in experiments using a surface force apparatus [60], but a transition to a continuous slip without wear was noted at much higher velocities. Thus, to compare this data with the AFM data, it is necessary to increase the scan velocity of AFMs.

Does this periodicity of the SS effect signify that the probe atoms form a structure commensurable with the atomic structure of a sample? Even for probes with a disordered atomic structure, the periodicity of lateral forces corresponds to the translational symmetry of the sample. In typical experimental situations, both lateral and longitudinal deformations of a cantilever generally take place, but the latter may also be determined by the change of the normal force. Therefore, there always exist a relation between the corresponding signals in the lateral and normal modes. If this relation is not controlled, it can totally distort the results of measurements.

Tomlinson [61] was the first to raise the question of the role of atomic structure in the relative movement of contacting surfaces. Since that time many authors have attempted to explain the SS effect using modernized classical notions of Tomlinson and the molecular dynamics method (see references in papers [3, 4] and Section 5). In the present-day models developing these ideas, a probe is considered as a point particle with a point mass without any internal degrees of freedom [56, 57], or allowance is made for its multi-atomic structure [62, 63]. A simplified, but visual picture of the SS effect is as follows.

Initially the probe is at a point of the minimum of the potential energy of the 'probe – surface' system. The interaction between the probe and the surface is defined by a periodic potential reflecting the translational symmetry of the atomic structure of the surface. Essential to the model is the assumption that adiabatic conditions are fulfilled at each step of probe movement. The lateral loading of the contact caused by cantilever scanning results in storing energy in the form of the elastic energy of the contact, the cantilever and the sample (see Fig. 4b and Fig. 13). The relative movement of the probe and the surface begins at the instant when the stored energy is sufficiently large that the probe can 'jump out' of a potential gap and fix itself at another point of the surface. Then the system relaxes, and excess energy rapidly dissipates from the contact area via the electron – phonon subsystem. The dissipation time is very small, since the characteristic velocities of electrons and photons are many orders of magnitude higher than the typical velocities of AFM probe scanning ($10^{-7} - 10^{-4}$ m s^{-1}).

As follows from experiments and model calculations, in order that instability related to the SS effect be observed, it is necessary to use the combination of a 'soft' cantilever and a 'stiff' surface strongly interacting with each other. In this case, the softer the contact, the more energy dissipates. However, in the models the possible mechanisms of energy dissipation in which the friction force is proportional to the velocity are not taken into account. Slip without friction was theoretically substantiated in works [62, 64] when the above conditions were not fulfilled.

The oscillator model adequately describes the SS effects only under the condition of critical damping of a cantilever. This is its weak point when the large elasticity of cantilevers is taken into account. To eliminate this contradiction, Johnson and Woodhouse [65] introduced the contact stiffness and found a relationship between the effective stiffness of the 'cantilever – surface' system and the amplitude of the periodic friction force (for more details, see Section 5.2).

On the whole, the weakest point of this theory is inconsistency between the point oscillator model and the actual situation with the AFM probe when the contact area measures tens of nanometers and hence involves many atoms. In this case, as follows from calculations [66], at different positions of the apex of a diamond probe on the graphite surface (for a real-size probe with a radius of curvature of 5 – 15 nm) the change of the potential energy of the system after relaxation does not exceed 0.2 eV. Therefore, one cannot say that the probe jumps from one position of energy minimum to another. Experimental evidence lies in the fact that the period of the SS effect coincides with the period of a surface atomic structure. Thus, in the contact lateral mode of an AFM we must not speak of 'true atomic surface resolution', as in the modulation mode [38], but about 'atomic contrast'. This is supported by the fact that the point atom defects of surfaces are not resolved in the contact mode.

A more realistic geometry of the 'equilibrium' contact area corresponds to Fig. 4a, and any sharp lateral twisting of the cantilever (Fig. 4b) is connected with increasing energy. To put it otherwise, each position of the probe on the surface corresponds to the minimum of energy.

The molecular dynamics calculations also predict the presence of the SS effect [67 – 69]. Landman et al. (see Ref. [67] and references therein) and Sorensen et al. [68] studied Si (probe) – Si (surface) and Cu (probe) – Cu(111) (surface) contacts, respectively. Friction without wear was observed at small loads. A decrease of the friction force with increasing scan velocity was also noted. These results will be discussed more comprehensively in Section 4.3. Here we only point out that the most serious objection to the results of the MD calculations connected with the interpretation of the SS effect is that the range of velocities used in these calculations includes velocities ($1 - 2000$ m s^{-1}) considerably greater than the scan velocities in AFM. Another problem, also relating to quasi-static models, is the lack of information about the actual structure of the probe and the lack of control over it. Nevertheless, the numerical MD experiments have enriched our understanding of structural changes taking place in the contact area.

In my opinion, a clear-cut distinction needs to be drawn between conservative lateral forces acting on the probe and

dissipative forces (see Section 4.4). When considering the probe movement corresponding to the friction loop shown in Fig. 3, we are dealing with the maxima of a static force determining the onset of slip. However, we have no knowledge of the atomic structure of the contact area at the corresponding moment and cannot answer the question of whether there is any motion of atoms within it. The authors of work [35] believe, for example, that at the periphery of the contact restricted slip of atoms takes place even at very small lateral forces. Hence, the lateral force observed cannot be totally assigned either to a dissipative force or to a conservative one. It is possible that it is a combination of both components.

As was mentioned in Section 2.5, experimental information obtained with the use of an AFM for lateral forces (Fig. 3) is still not finally understood. This concerns, for example, the interpretation of the fine structure of friction loops. The discreteness of the small variations of the lateral force observed in experiments most likely reflects the discreteness of breaking individual adhesive bonds that is analogous to breaking the bond in the vertical direction in the lowering-lift mode of the probe [70].

As to the shift of the lateral contrast on reversing the direction of probe movement (Fig. 3), there is nothing out of ordinary in it, since the contrast does not directly display an atomic structure. For a probe in the extreme right position (the upper curve in Fig. 3) the system is ready to make a microslip, therefore it does not matter whether the probe will continue to move to the right or reverse its direction — in either case the force magnitude must further decrease (that is actually observed). As a result, after a sharp decrease of the lateral force in the initial stage of the reverse movement of the probe this force turns out to be close to zero, the contact gets 'unloaded' and only then a new increase of the lateral force begins, the force continuing to increase until the next slip cycle begins. This shows once again that sharp changes of the lateral force are irreversible and connected with the dissipative character of the slip process.

The atomic periodicity of the SS effect is qualitatively explained by the model of making and breaking adhesive bonds (see Section 4.4). At each position of the probe on the surface, the 'spot' of contact covers a particular area of the surface, and for a spot of a specified form the number of surface atoms beneath it varies depending on the lateral coordinates with the surface lattice period. This was demonstrated, for example, for one- and multilayer nanowires in last year's work by the author of this review [53]. If the probe is located at the point corresponding to the minimum number of adhesive bonds in the vicinity of the contact spot boundary, then for an abrupt microslip (over a small distance in comparison with the surface lattice period) the dissipative friction force will be minimal, since the number of broken and newly-made adhesive bonds is moderate, and small discrete jumps observed as a fine structure of the lateral force (see Fig. 3) are not accompanied by the loss of stability of the system, which continues to accumulate energy. On the contrary, in the position corresponding to the maximum number of bonds along the spot boundary, the breaking of these bonds because of the microslip with a subsequent sharp decrease of the lateral force at the cantilever becomes catastrophic in character — and the probe gets away. Old adhesive bonds (behind) are broken, reducing resistance to the onward movement of the probe, and new bonds, made ahead, draw it forward. The character of this movement is adequately represented by a model in which atoms-magnets are stacked on the surface in the form of a regular grid and have a vertical degree of freedom, and a probe having a flat form (with the same magnets on its surface) is fitted to a pendulum whose axis moves with a constant horizontal velocity. This model allows one to visualize the atomic SS effect on the macroscopic level.

On the whole, many fundamental aspects of the SS effect still remain to be seen. First and foremost there is no clarity in determination of concrete experimental conditions under which the SS effect must be observed, in concrete definition of the mechanisms of dissipative losses, in the problem of the periodicity length and so on. The latter is especially urgent for alkaline-haloid crystals, for which slips both over the lattice period and over one-half the lattice period were observed.

3.2 Adhesion effects

Adhesion effects are obviously essential to the problem of atomic friction, since they determine the area of the contact and the interaction of the probe with the sample [6]. Adhesive forces can be directly measured with the help of an AFM using the lowering-lift mode or the measurement of the 'friction force – loading force' dependences [35, 42, 43, 72]. In the event that contact mechanics are used for data interpretation, two main parameters being determined in these measurements are the shearing stress and the adhesion work. The shearing stress is directly proportional to the critical lateral force causing probe slip in the stick-slip mode. The adhesion work is equal to the specific energy (per unit area of a contact) required to break the contact. By definition, the adhesion work is

$$\gamma = \gamma_1 + \gamma_2 - \gamma_{12}\,, \tag{3.1}$$

where γ_1, γ_2, γ_{12} are the specific surface energies of the probe and the sample and the interface energy of the contact, respectively.

The basic problems to be solved are concerned with the dependence of these quantities on the atomic structure of the contact, temperature, external pressure, chemical composition and so on. A distinction needs to be drawn between 'dry' vacuum conditions and the more complicated case of a 'wet' surface when intermolecular forces may considerably vary owing to the presence of molecules of a solvent or a dissolved substance.

In the case of 'dry' friction, the adhesion work is determined by the force of detachment of an AFM probe from a surface. The force of detachment is negative in sign and corresponds to a force applied to a cantilever which is necessary for surface separation. For elastic adhesive contacts in the case of a parabolic-profile probe with a radius of curvature R, the Johnson – Kendall – Roberts (JKR) theory [73] (for more details, see Section 4.1) gives the following expression for this force:

$$P_0 = -1.5\pi R\gamma\,. \tag{3.2}$$

The JKR theory describes the elastic contact of soft materials with a strong short-range (attractive) adhesive interaction. The contact of stiff materials with long-range attraction is best described by the Deryagin – Muller – Toporov (DMT) theory [27]. In this case the numerical factor in formula (3.2) is replaced by 2.

One further formula relates the remanent friction force F_0 at the point of probe detachment and the adhesion work. In

the JKR approximation they are related by the following formula:

$$F_0 = \pi\tau\left(\frac{9\pi R^2\gamma}{8E'}\right)^{2/3}, \tag{3.3}$$

where τ is the shearing stress, $E' = (1-\eta_1)/E_1 + (1-\eta_2)/E_2$, and $E_{1,2}$ are the moduli of elasticity of the components. In the DMT theory $F_0 = 0$, and the force of detachment corresponds to the Van-der-Waals attractive force and in the case of a spherical probe is equal to

$$P_0 = \frac{HR}{6h^2}, \tag{3.4}$$

where H is Hamaker's constant, R is the radius of the probe, and h is the distance between the probe and the surface at the instant of attachment. Typical values of h and the H constant lie in the ranges 0.2 to 0.3 nm [73] and 0.6 to 2.5 eV, respectively.

Using formulas (3.2), (3.3) and the measured values of the P_0 and F_0 forces, the authors of work [40] found that $\tau \propto \gamma^{0.44}$ for the interaction of a platinum-coated probe with mica (under high-vacuum condition). In this case a progressive decrease of these forces from one cycle to another was observed (Fig. 5). The authors believe that these peculiarities are connected with chemical or structural changes in the contact area induced by probe scanning. It is also assumed that these variations of friction and adhesion may be determined by the change of the character of commensurability of contacting surface structures.

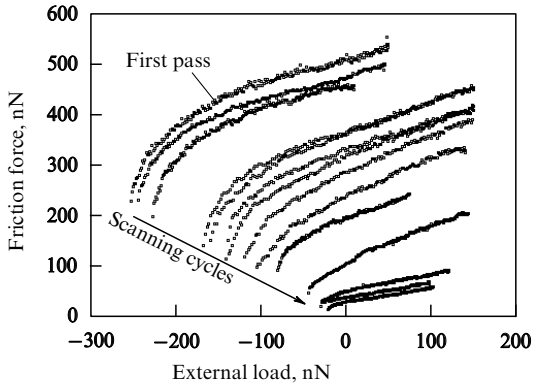

Figure 5. Progressive decrease of the adhesion energy and the shearing stress when measuring experimental 'friction force – loading force' dependences in the case of scanning by a platinum-coated probe over a mica surface in vacuum. After each scan cycle the adhesive force of detachment and the shearing stress are diminished. This means that friction and adhesion are sensitive to the changes of structure and/or chemical interactions in the contact area. Such behaviour takes place independently of the changes of the probe shape. (Reproduced with the permission of Salmeron [43], copyright of the American Physical Society, 1998.)

The weak dependence of the shearing stress on the value of the adhesion work seems to be highly unusual, since more frequently a linear proportionality between these quantities is observed (in the absence of wear). The simplest model providing an explanation for this dependence is the 'cobble-stone road' model equivalent to the Tomlinson model. The slip of surfaces in contact is considered by analogy with the movement of a carriage wheel. At rest the wheel lands in a hollow formed by cobble-stones, and to set it in motion, it is necessary to apply a lateral force large enough for the wheel to get out of this hollow. In this model the role of attractive surface forces is played by the force of gravity. For an atomic-smooth surface, atoms correspond to the cobble-stones, but the picture considered will be the same for the contact structure shown in Fig. 4a. Experiments carried out with the use of an SFA on surfaces covered by hydroxyl groups and the molecular layers of liquids support this model [4]. In these works it was also shown that for the systems of chain molecules the adhesion work increases when the surfaces are brought into contact. Besides, hysteresis of the area of contact in the processes of bringing together and separating the surfaces is observed, and the friction force increases with increasing hysteresis.

Israelachvili proposed a theory [74] establishing a link between friction and adhesion which is determined by the internal structure of molecular structures (hydrocarbons), but for 'dry' tribocontacts, no adhesive and friction hysteresis should be observed [43] in contrast with the predictions of this theory.

Another model establishing a link between the shearing stress and the adhesion work (in the case of 'dry' contacts) was proposed in works [75] (for more details, see Section 4.4). Figure 6 shows the correlation dependence between the macroscopic values of the surface energy of metals and some other solids and the product of the shearing stress by the atomic radius plotted on the basis of the existing experimental data for homogeneous contacts [75]. As was mentioned in Section 2.4, the shear modulus is directly proportional to the shearing stress, therefore, it is believed that G and τ vary in concord, and Fig. 6 reflects equally the correlation of τ and γ. Fig. 6 shows that one can recognize two groups of materials with different coefficients of proportionality between τ and γ, or, alternatively, this dependence is nonlinear. In the latter case it is nearly quadratic: $\tau \propto \gamma^2$.

In the author's opinion particular emphasis should be placed upon the paradoxical results of comparative analysis of a correlation between the value of the adhesion work measured with the use of an AFM and the expected macroscopic values of this quantity, on the one hand, and an analogous correlation for the values of the shearing stress, on the other hand. For example, for Si (probe) – $NbSe_2$ (sample) contacts experimental values of the shearing stress,

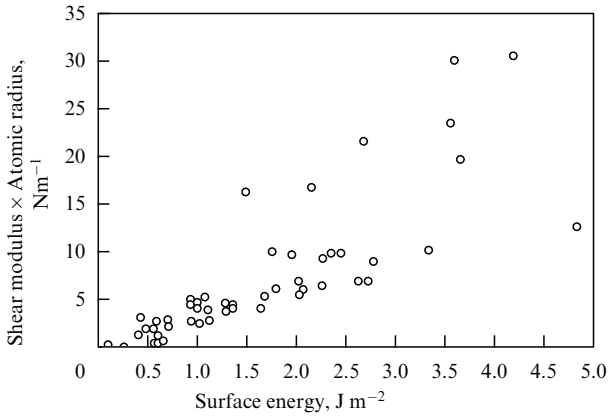

Figure 6. Correlation between the product of the macroscopic shear modulus by the atomic radius and the surface energy of solids. The values of the surface energy are reduced to 0 K. (Extended version of a similar diagram from Ref. [75].)

obtained with the help of the AFM at different radii of curvature of the probe, fall in the range 0.61 to 0.66 GPa, that is, are close to the value of τ in the macroscopic case, 0.57 GPa. At the same time the values of the adhesion work ($0.65-0.1$ J m^{-2}) seem to be too small in comparison with its macroscopic values. For example, for hard silicon the surface energy is close to 1.8 J m^{-2}, for hard niobium it approximates 2.5 J m^{-2}. For selenium no data are available, however, it may be assumed that for hard $NbSe_2$ its value ranges from 0.3 to 1 J m^{-2}, since $NbSe_2$ has a layered structure similar to that for graphite, and for graphite $\gamma \approx 0.33$ J m^{-2}. Thus, for the Si–$NbSe_2$ contact one would expect $\gamma_1 + \gamma_2 \approx 2.1-2.8$ J m^{-2}. Therefore, to obtain these extremely low values of the adhesion work observed, it must be assumed [according to formula (3.1)] that the phase interface energy γ_{12} is practically equal to $\gamma_1 + \gamma_2$. Such large values of γ_{12} are, in turn, indicative of a dramatic rearrangement of the atomic structure of the interface boundary that, however, seems to be highly improbable in the case of the contacts of hard materials. In particular, for the contact of homogeneous bodies we have $\gamma_{12} = 0$.

Thus, the assumption that the orders of magnitudes of the macroscopic characteristics of materials are retained when going to a nanoscopic scale is not so apparent. An analogous conclusion follows from the analysis of the values of the adhesion work in other experiments (see, for example, the data of Table 1 in Ref. [3]).

Considerably more complex adhesion effects are observed in the case of 'wet' tribocontacts. Many were studied by way of measuring approach-distance curves [4]. The use of the AFM method in this case appears to be particularly promising, since solvation forces are the least understood. Measurements of these forces on the surfaces of graphite and mica coated with *n*-dodecanol and octamethylcyclotetrazilocsane were conducted using an SFA [76]. The interpretation of solvation forces is easier when liquid is 'clamped' between two macroscopically-smooth plates, but not so apparent when one of theses plates is replaced by an AFM probe. The molecular dynamics simulation of solvation forces for a 'nickel (probe)–gold' contact with a hexadecane interlayer was performed in work [77].

The authors of work [78] studied the relation between adhesion and friction for a silicon nitride probe on an Au(100) surface coated with chains of built-in organic molecules (alkanes). In these experiments a linear correlation between the macroscopic values of the surface energy determined from the contact angle of wetting, and friction forces was found.

Owing to the small area of the contact made between an AFM tip and a surface, it is possible to observe the 'quantization' of adhesive forces. In work [79] this effect was found when measuring adhesive forces between a silicon nitride probe and a glass surface coated with water. Discrete jumps of adhesive forces of the order of 1 pN were observed in the approach-distance curves. The authors succeeded in revealing the thermomechanical fluctuations of the coordinates of the probe corresponding to its different metastable positions. These fluctuations appear because of exfoliation of water and/or hydrate ions on the surface of ionic crystals. In these experiments, the probability of localization of the probe at a distance s from the surface is determined by the Boltzmann distribution

$$p(s) \propto \exp\left[-\frac{V(s)}{k_B T}\right], \tag{3.5}$$

where $V(s)$ is the potential energy, k_B and T are the Boltzmann constant and the temperature, respectively. The measured minima of $V(s)$ obtained by way of inverting formula (3.5) have a periodicity of $0.15-0.3$ nm that is comparable with the dimensions of water molecules.

A great number of other adhesion effects follow from the MD simulation [4, 18, 69, 80–83]. Among these are the formation of adhesive avalanches [84], the plastic creep of probe material with the formation of crowdions and the generation of dislocations [82, 85], the vibration mechanism of compression and disruption of metallic nanoparticles at inelastic impact [82] and so on. However, there are some contradictions between experiments and the results of the MD simulation. For example, in contrast with the MD calculations the hysteresis of adhesive forces is not always found in experiments.

In connection with tribological problems, it should also be noted that in numerical MD experiments there is evidence for the existence of a differential strength effect (for more details, see Ref. [82]). The authors argue that the strength of materials for uniaxial compression is much higher than for stretching. If such an effect exists, the low strength of phase boundaries may be observed.

3.3 Chemical effects

Tribochemical effects on the macroscopic level were adequately covered in monograph [86], however, the use of AFMs opens up new interesting possibilities [3, 6, 87].

Friction can both stimulate and suppress chemical processes, and these latter, in turn, affect friction that is sensitive to the chemical composition of the contact area. The chemical-composition dependence of normal and lateral forces may, in particular, be used to obtain the relevant images and to study the chemical reactivity of a surface.

Marti et al. [13] have shown that the measurements of lateral forces between a silicon nitride probe and a quartz surface placed in a solution are dependent on the hydrogen index of the solution. The authors attempted to relate the measured value of friction to the adhesive hysteresis observed in experiments with the use of an SFA [60]. In accordance with theory [74], in the case of 'wet' contacts, adhesive and friction hysteresis is due to the influence of complex processes, such as the reorientation, interdiffusion and intertwining of the chain molecules of hydrocarbons. Adhesive hysteresis takes place for 'dry' contacts as well (see Fig. 5 and Ref. [43]), however, in this case the theory proposed in work [74] is not appropriate.

Friction hysteresis on the wet surfaces of alkaline-haloid crystals was observed by Carpick et al. [39]. The measured dependences of the friction force on the loading force for the KCl and KBr surfaces are presented in Fig. 7. They differ radically (in a qualitative sense) from analogous dependences for elastic contacts (see Figs 5, 12, 13). To interpret these curves, the authors hypothesize that the contact area undergoes a structural modification. Analogous (linear-type) dependences were observed for gold, silicon nitride and organic films [88]. It is possible that such (linear) dependences are specific for tribochemical wear. In the case of a $NaNO_3$ wet surface in contact with a probe, the splitting of diatomic steps into monoatomic ones and a material transport from steps to above-spaced terraces were noted [89]. The influence of humidity on the force interaction of a probe with a surface was also studied [16, 17].

Phenomena of tribochemical degradation were noted in the cases of the MoS_2 surface as well as diamond-like film

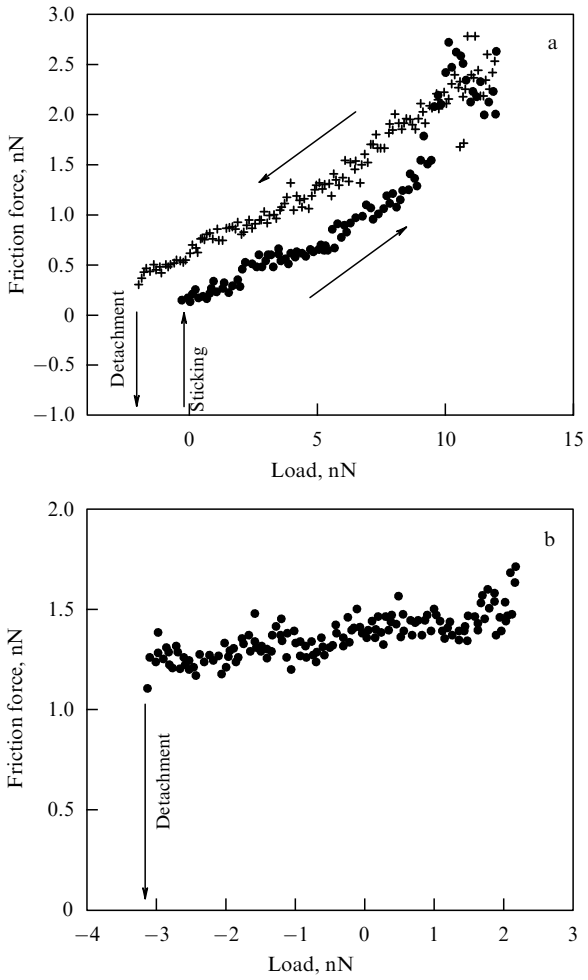

Figure 7. 'Friction force – loading force' dependence for KCl (a) and KBr (b). In case (a) the friction force was varied over a relatively wide range. The friction force increases in a gradual manner until the loading force becomes equal to 5.5 nN, then a sharper increase is observed. At loads above 9 nN, irregular fluctuations of the friction force are observed. In this case the friction force exhibits hysteresis as the load is decreased and does not revert to its original value. Case (b) corresponds to the regime of small loads. A considerable remanent friction force at the point of detachment of the probe from the surface and its weak linear increase with increasing load are worthy of note. Such a dependence differs sharply from analogous dependences in the case of elastic contacts (see, for example, Fig. 5). (Reproduced with the permission of Salmeron [43], copyright J C Baltzer AG, 1998.)

coatings, whereas for the diamond – diamond contact, on the contrary, the presence of humidity results in a decrease of it (see Ref. [6]).

Tribochemical processes have already found use in nanolithography (see work [90] and references therein), since the regions of tunnelling contacts with a passivated silicon surface undergo selective oxidation. On the whole, the study of tribochemical processes on a nanoscale is still in its infancy.

3.4 Formation of dents and scratches, wear

Friction without wear is a consequence of the elasticity of a contact, if the damage-formation threshold is not reached. Energy may also transform into heat in the process of plastic deformation, therefore, the latter plays an important role in determining the tribological characteristics of materials.

As was already mentioned, images obtained in the contact mode of an AFM cannot reveal the formation of point defects, therefore, so far it is unclear whether they are formed or not in the process of scanning in the regime of small loads. If these point defects occur, they must markedly affect friction forces. This problem needs special theoretical consideration.

Wear of the probe and sample materials was observed in many experiments (see discussion in Ref. [3]). In some cases, after scanning part of surface, damage was observed at loads above a certain threshold, in other cases the process of wear became tribochemical in character [91]. Of course, a distinction needs to be drawn between wear (or degradation) of a surface in vacuum conditions, on the one hand, and in atmospheric conditions, when the processes of oxidation are dominant, on the other. In this section we discuss wear of clean surfaces only.

As one would expect, the depth of scratches resulting from nanoindentation increases with increasing load. The observation and control of this process for changing loading forces allow one to study the mechanisms of material fatigue and to determine the resistibility of ultra-thin coatings to wear. Since AFM methods make it possible simultaneously to conduct measurements of the indentation depth and the value of the normal force, outstanding possibilities are opened up for the investigation of plastic deformation of materials and surface coatings. Such experiments have revealed an increase in the shearing stress and microhardness of gold films by an order of magnitude in comparison with macroscopic samples. However, in some works (see, for example, Ref. [92]) it was noted that hardness increases with increasing load. Using AFM, one can transfer a nanostructural material from one surface onto another, as was demonstrated, for example, in the case of fullerene films.

Friction and wear under higher loads can be effectively studied with the use of the technique of controlled multiple slip along a prescribed direction [24]. In Ref. [24] the formation of scratches and the adhesive strength of silicon nitride, carbon nitride and diamond-like coatings 20 nm thick in the process of indentation were investigated. A three-cornered diamond indentor with a radius of curvature of 50 nm at loads from 0.2 to 0.8 mN was used. In the initial phase of slip, the main mechanism of wear was the 'ploughing' of the surface. However, on increasing the number of scans or the normal load, the process of scratch formation began to predominate. Such experiments are of great interest for testing the scratch theory.

The appearance of point defects in the process of scanning an AFM probe at small loads was first predicted by Schluger et al. [93] who simulated the interaction of an MgO probe with newly-cleaved surfaces of NaCl and LiF. It was assumed that a chemically active OH^- group is localized on the apex of the probe. On subsequent simulation, the formation of vacancies and interstitial atoms on the surface of the sample as well as the movement of individual ions through the contact area.

The simulation of atomic wear was performed by many authors [67 – 69, 82]. In these works the formation of adhesive avalanches [82], the plastic creep of atoms into interstitial positions and the extrusion of material in the vicinity of the probe surface [83], and the formation of dislocations [69, 94] were studied. For example, a simulation procedure for the contact of a Ni (Au) probe with the Au (Ni) surface shows the presence of an instability as the probe approaches the sample to a distance of about 0.4 nm [4]. In the vicinity of the corresponding point, strong adhesive coupling occurred accompanied by sudden 'wetting' of the nickel by gold atoms. Lifting the probe from the surface resulted in a

considerable inelastic deformation and disruption of the sample in the contact area [69].

Some new peculiarities of adhesive wear were observed in works [82] for a W (probe) – Fe (sample) system. The authors note several stages of this wear: the displacement of surface atoms ahead of a moving probe, phase mixing, the ordering of probe atoms and their 'sticking' to the surface of the sample. Simulation for ionic crystals (CaF_2) and silicon crystals has revealed a surface-material shift and inter-phase transport [95] as well as the fragmentation of material because of the impact of a probe [96]. The simulation of nickel probe slip over the relatively soft copper surface (whose structure is incommensurable with the structure of nickel) [69] has shown the presence of a peculiarity of stick-slip cycles lying in the fact that each cycle includes two different processes accompanied by structural transformations: in the first stage of slip one layer of nickel atoms changes its structure to match the copper surface structure, and then, in the second stage, two layers form a new structure (see Section 4.3). Eventually, this results in wear, with a quasi-linear increase of the lateral force at small loads at the stick stage and a sharper drop at the slip stage. This is in qualitative agreement with experimental AFM data (see Fig. 3). At large loads, the stick-slip effect becomes less regular.

3.5 Interfacial lubrication and shear ordering of film structures

Among theoretical problems relating to nanotribology, the problems of interfacial lubrication are most complex, since the correlation of the properties of lubricating materials with adhesion and friction initiate a wealth of new physical effects [6]. There is wide use of lubrication coatings based on self-supporting multimolecular liquid layers. A more effective method consists in coating the contacting surfaces with chain multilink molecules [4]. Such self-ordering monolayers can be obtained by deposition of Langmuir – Blodgett (LB) films or by chemical 'integration'. Besides, in recent years fullerenes and nanowires have attained widespread application as lubricants.

An extended discussion of the application of AFMs and SFAs in studies of lubricating coatings and their structures on shearing and compression can be found in reviews [3, 4], therefore, we dwell only on the most interesting details of the relevant experimental results.

The structure of ultra-thin films strongly depends on the intermolecular forces within a film and its interaction with the substrate. As noted in work [4], the influence of two solid surfaces adjacent to the film leads to a vastly greater diversity of inter-phase properties in comparison with the case of only one surface. If the interaction of a solid surface with a liquid interlayer induces the coagulation of the latter and the film periodically melts and congeals in the process of slip, then we are dealing with slip – stick friction of surfaces. Sticking corresponds the coagulation of the film and gives rise to a static friction force. Slip arises when the melting of the film is induced by shear, with the result that the friction becomes kinetic in character.

The relative value of intermolecular forces and film-substrate interaction forces depends on the length of the links of chain molecules or on the number of CH_2 (n) groups entering into their composition [3]. It is expected that for $n < 10$ Van der Waals forces between the molecules and a substrate are dominant, and for $n > 12$ the covalent interactions of the 'heads' of individual molecules with one another are more essential. For self-ordering silane-type structures, it is necessary to take into account both the interaction with the substrate and the interaction of the chains of individual molecules. In this case the formation of 'bridges' Si – O – Si linking adjacent molecules distorts the structure of the head parts of the molecules adjacent to the substrate and results in the disappearance of long-range order in the film structure.

Using the modulation AFM mode, Overney et al. (see Ref. [97] and references therein) observed a correlation between friction and the elastic properties of films. Under load a softer film forms a contact with a larger area and, hence, with larger friction. The molecular structures of films essentially depend on the applied pressure and temperature. For sharper probes (with a radius of curvature of about 100 nm), pressures reach values of the order of several GPa, therefore, such probes easily pierce films and displace molecules in the lateral direction. Pressures of the order of 10 – 200 MPa cannot produce marked structural changes, and the molecules remain in a more or less normal state, bearing the load applied to the cantilever, and the probe slips over the 'heads' of the molecules. The critical value of the loading force P_c which can produce structural changes in films increases on increasing the radius of the probe. For thiol molecules on a gold surface the original structure of the film is regained after unloading, but for silanes this is not the case.

One can provide a simple explanation for the last-mentioned effect considering the elastic deformation of a film, on the one hand, and the increase of the area of contact on compression, on the other [3]. The process of deformation causes the absorption of energy, whereas the increase of the area of a phase interface, on the contrary, provides the generation of energy. The reversibility of the transition for thiol films (after unloading) is connected with the relatively small number of molecules displacing from a region under the probe in the surrounding medium, since they possess finite lateral compressibility. For silane films on mica, on the contrary, deformation induced by the probe and the displacement of molecules cause the irreversible disruption of Si – O – Si bridges, therefore, the original structure is not regained.

Dynamical structures occurring in the process of lubrication slip of surfaces carrying layers of surfactants and/or polymers depend on the slip velocity and temperature. This fact is known as the temperature-time superposition principle. High slip velocity and low temperatures are favorable to the coagulation of the films, whereas low velocities and high temperatures cause them to melt [4]. As a result, solid films exhibit interrupted slip – sticking with high friction, and liquid ones shows superkinetic slip of a viscous character with low friction. An intermediate case corresponds to amorphous structure films with high friction because of the entangling of molecular chains. The results of simulation of these structural changes and phase transformations on the atomic level are in gratifying agreement with experimental results.

Krim and Chiarello [98] studied the influence of structural transformations on the damping time of motion of adsorbed krypton films using the quartz crystal microbalance technique. A long slip time is obviously determined by low friction. The slip time for solid monolayer structures was found to be larger than that for liquid structures. Being in a solid phase, krypton atoms are 'locked' in a structure incommensurable with the structure of substrate atoms (Au). Therefore, for lack of stable localisation (with a minimum of energy relative to the substrate), the Kr films

slip with low friction. For commensurate structures, on the contrary, the friction force turns out to be many orders of magnitude higher [62]. This behaviour is opposite to that which is inherent in the above-considered friction of the layers of chain organic molecules.

A number of analogous results relating to the friction of adsorbed films were obtained in numerical MD experiments. In particular, the existence of transitions from film structures incommensurable with substrates to commensurable ones, strongly affecting the value of the friction force, was confirmed. For example, Tamura et al. [99] considered a realistic model of friction between talc (001) surfaces (at a pressure of 1 atm and a temperature of 300 K). The total number of atoms was 570. The authors took 7 atomic layers for each film and imposed a periodic boundary condition in the plane of slip (xy). Setting the velocity (50 m s^{-1}) of the atoms of the upper film (or of a part of this film), they analyzed the movement of the centre of mass. It was found that friction is high in the case of commensurable structures with zero angle of disorientation and low for incommensurable structures with an angle of disorientation of 30°. The relation of the friction force with the fluctuations of the interphase interaction potential was also found.

In work [100] the MD simulation of the motion of a monoatomic adsorbed layer on a crystalline surface (for a conventional model situation) was conducted. The model sample included 5760 atoms, and the temperature was fixed below the melting point. The main result of this work was the detection of the effect of 'locking' motion for a short time interval (about 0.1 nsec), with external forces being unchanged. A necessary condition for 'locking' is the presence of incommensurability and structural degeneration which promote the reconstruction of the film structure and its transfer to another equivalent modification.

The role of electron and phonon excitations in the problem of the dynamical friction of adsorbed films has been studied theoretically by many authors. We will revert to the discussion of these questions in Section 4.5.

3.6 Metallic nanocontacts

In a number of works, synchronous measurements of loading forces and electric current in conducting metallic nanocontacts between a probe and a sample fabricated from the same material were performed. The measurements were conducted both at room temperature under atmospheric conditions and in high vacuum [70, 101]. Discrete jumps of the conductivity of the nanocontacts corresponding to the relaxation of the forces of probe detachment from the surface were measured. The value of each jump of conductivity was of the order of the value of the conduction quantum $2e^2/\hbar$ and each jump of the force was $\Delta F = 1.5 \pm 0.2$ nN. Such changes of conductivity and the force of interaction would be expected as a one-atom contact is disrupted (see Section 4.3). Jumps of conductivity resulting from the disruption of metallic tunnelling contacts were also detected with the use of STMs.

The existing theoretical explanation of the discrete change of conductivity relates the mechanism of this effect with the atomic rearrangement of the contact area. This rearrangement includes the stage of elastic expansion and the stages of plastic creep and disruption of contact bridges observed with a periodicity of the interlayer distances in a forming contact bridge. The formation of extended bridges between the probe and sample leads to hysteresis of the 'force-load' dependence in the lowering-lift mode. Moving the probe away from the surface causes considerable deformation of the sample with counter movement of layers of the probe and sample materials adjacent to the contact as well as the formation and disruption of a contact bridge. Hence, the hysteresis of the 'force-load' dependence is a consequence of the disruption of the sample. This conclusion is supported by the MD simulation [69].

This picture is readily illustrated with the example of a spoon slowly being pulled out from half-candied honey. In the initial state (when the spoon is dipped into the honey) the honey surface is smooth and its grainy ('atomic') structure is not seen. On the contrary, when the spoon begins to detach, we can clearly see a layered structure of individual 'grains' in the contact bridge (stream) connecting the spoon with the bulk of the honey. In this case the variations of the velocity of the slowly flowing stream associated with the disruption of liquid interlayers between the individual grains of honey are visible.

A result of great importance, obtained in experiments [70, 101], is that the value of the contact stiffness turns out to be comparable with estimates following from the macroscopic contact theory (Fig. 8). In the case when the voltage across the contact is constant, current and contact conductivity turn out to be proportional to the area of the contact for an arbitrary conduction mechanism [3, 43]. This allows one to use the measurements of current and conductivity for relative calibration of the area of a nanocontact.

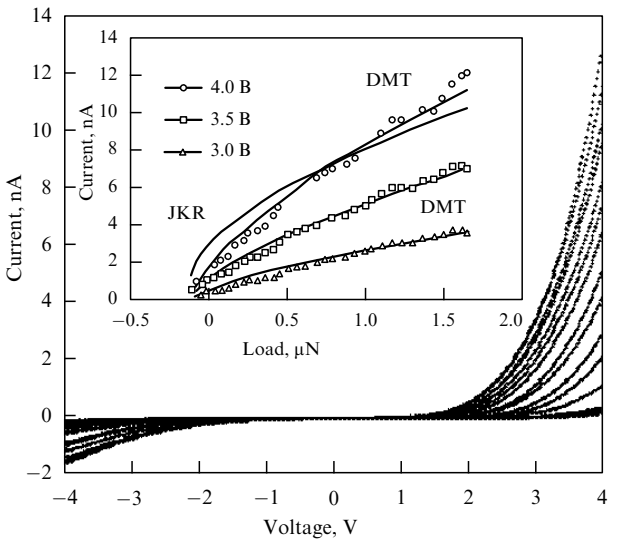

Figure 8. Set of current–voltage characteristics for tunnelling current versus loading forces (up to 1.7 μN) measured in the process of displacement of the sample (only every seventh curve is shown). Inset: tunnelling current through the contact as a function of the applied load at a constant voltage. One can recognize that the experimental values of the tunnelling current (proportional to the area of the contact) are in good agreement with the DMT theory. The JKR approximation (the corresponding curve is shown only for the first set of measurements) obviously inadequately describes this stiff contact (tungsten carbide – diamond). (Reproduced with the permission of Salmeron [72], copyright of the American Physical Society, 1998.)

3.7 Friction of films adsorbed on the surfaces of superconductors

In a recent paper [18] Krim et al., using the QCM technique, found a sudden decrease (by about one half) of the dynamical friction force acting on the layer of nitrogen

molecules physically adsorbed on the surface of a lead film as the temperature was decreased below the superconducting transition point of lead. Persson and Tosatti [102] discussed conceivable physical reasons for this effect associated with an electron contribution to dynamical friction.

In their experiment a lead film with an adsorbed layer of nitrogen molecules (1.6 ML in thickness) cooled below $T_c = 7\,\mathrm{K}$ was used. The sharp jump of the quartz-oscillator damping time observed is obviously determined by the transition of lead into the superconducting state. Analysing the role of electron friction, the authors of work [102] note that according to the existing notions (at normal temperatures) such a sharp change in friction should not to be observed because of the continuous change of the number of electrons going into the superconducting condensate, and this is inconsistent with experiment.

At these temperatures, the adsorbed film of nitrogen molecules must be solid and is likely to have a structure incommensurable with the substrate structure. Such a structure must exhibit low friction. However, there is no clear reason for the fact that the coagulation of the film takes place just at the superconducting transition temperature.

Some considerations can be applied to the role of fluctuation-electromagnetic friction (see Section 4.5). Taking into account the fact that in the process of interaction of a krypton film with lead (in the normal state) the absorption of electromagnetic waves in the frequency region near 10^{12} Hz, corresponding to the energy gap of lead, contributes essentially to friction (giving about one-half of the total), one can assume that the normal-superconducting transition of lead will result in decreasing friction.

In summary it should be said that even at normal temperatures the relation between different contributions in dynamical friction continues to remain the subject of intensive discussion (see Section 4.5). Therefore, the problem concerning the theoretical interpretation of the effect [18] offers considerable scope for different viewpoints.

3.8 Triboemission of particles, electromagnetic and acoustic waves

In work [15] an investigation of triboelectromagnetic phenomena for different slip contacts used in magnetic recording devices (for writing information on hard disks) was undertaken. The yield of charged particles and photons was measured in the process of slip of a diamond probe with a radius of curvature of 10 microns at a normal loading force of 0.5 N and a slip velocity of $2-7\ \mathrm{cm\ s^{-1}}$ (under atmospheric condition). The results of these experiments revealed a correlation pointing to an increase of the yield of particles with increasing conductivity of the surface material (Fig. 9).

To estimate the elastic energy stored in a typical nanotribocontact, one can use the following relationship of the Hertz theory: $U = 0.15P^{5/3}/R^{1/3}E'^{5/3}$ eV, where P, R, E' are measured in nN, nm and TPa, respectively. Then at $P = 100$ nN, $R = 50$ nm and $E = 0.1$ TPa one obtains a value of about 415 eV. On the other hand, the formation of scratches and adhesive processes occurring on the newly-cleaved surfaces of dielectric materials may be accompanied by the appearance of strong local electric fields capable of further accelerating charged particles.

One can assume that charged particles formed in the process of friction of a probe are capable of escaping from the surface and may be detected only in the event that the discharge time for arising electric fields is sufficiently long. For metals, this time is about 10^{-15} s, therefore, even fast electrons, having velocities of the order of the Fermi velocity ($2 \times 10^8\ \mathrm{cm\ s^{-1}}$), have no time to escape from the surface. Hence, the escape of positive and negative particles observed for metals is likely to be determined by the chemical reactivity of the impaired (by the probe) surface interacting with surrounding air molecules.

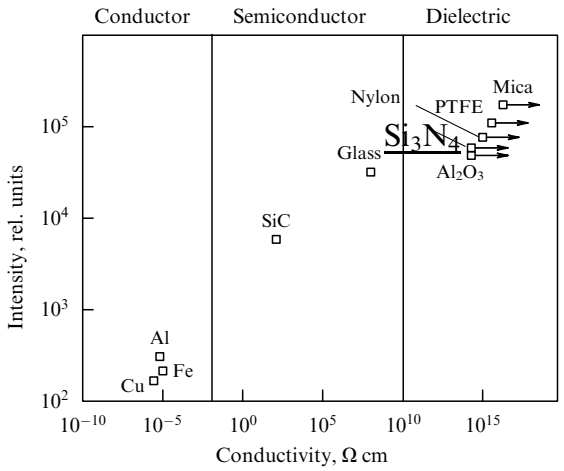

Figure 9. Correlation between the intensity of charged particles emitted from the probe–surface contact area and the conductivity of solids. The measurements were conducted in air for a diamond probe with a radius of 10 μm at a loading force of 0.5 nN and a slip velocity of 7 cm s^{-1}. The arrows show that the values of resistance are beyond the limits of the instrument sensitivity. (From work [15].)

For semiconductors and dielectrics this is not the case, and a considerable fraction of particles may escape from the surface in the process of field desorption or evaporation. These notions give a qualitative explanation for the observed dependencies of the yield of particles in the case of conductors and dielectrics (see Fig. 9).

Obviously, there is a need to conduct more detailed experiments of this type to determine the peculiar features of the corresponding mechanisms of emission in vacuum. First and foremost it makes sense to measure the energy spectrum of escaping particles. Assuming that the yield of particles is proportional to the area A of an actual contact, one can estimate a relative decrease of the yield when going from a micro- to a nanoscale. In the Hertz approximation, for the area of the contact we have $A \sim (PR)^{2/3}$, where P and R are the normal loading force and the radius of curvature of the probe, respectively. Then at $P = 100$ nN and $R = 30$ nm, one obtains that the yield of particles is of the order of 10^{-6} of that observed in work [15]. Such a yield can be measured with the use of more sensitive detectors.

The effects of electron nanotriboemission obviously have much in common with exoelectron emission observed in different conditions. The measurement of this emission is one of the promising methods for surface studies. The AFM method gives excellent possibilities to record the spectra of exoelectron emission, occurring on normal and lateral loading of nanotribocontacts, in synchrony with sample scanning. As far as is known, such measurements have not been conducted.

The authors of work [103] observed the acoustic emission occurring in the process of slip of magnetic recording heads in

the tapping mode. Such emission gives signals of contact of a probe with a surface (formation of scratches) [50].

High-speed processes taking place in the contact area may generate different types of radiation, therefore, it is advantageous to use the corresponding effects in studies of nanotribological actions on a surface.

In conclusion of this part of the review we formulate the most important problems of experimental character whose solution must refine the understanding of the physics of nanotribocontacts.

To obtain solid quantitative information using AFMs, it is necessary to perform *in situ* force calibrations taking into account concrete instrumental peculiarities, such as normal-to-lateral signal relationship, nonlinearity of piezoceramics, creep, hysteresis and so on.

One of the primary problems is the determination of the characteristics of a probe, its shape, structure and chemical composition. It is necessary to combine and apply different methods for determination and control of its form as well as the combinations of different materials and the geometry of contacts. In this connection the methods of determination of probe shapes and the area of contacts based on the measurements of contact conductivity and the yield of the inverse scattering of a low-intensity ion beam in Rutherford scattering are noteworthy. The unknown properties of probes can be revealed through comparative analysis of their characteristics. In this respect materials of considerable promise for probes are single fullerenes and nanowires.

It makes sense to conduct more detailed studies of the stick-slip effect and the mechanism of adhesive wear over a wider interval of slip velocities for different combinations of materials. There are a number of scantily studied aspects of this effect associated with the character of periodicity, the threshold of the slip start and anisotropy, the criteria of antifriction slip, the formation of point defects, the determination of the role of the structural commensurability effect and fluctuations of the phase interaction potential.

The fundamental processes of energy dissipation because of friction remain scantily studied. There is, in particular, a need for the determination of the peculiar features of the dynamical mechanism of electron (electromagnetic) and phonon friction. The mechanisms of noncontact dynamical friction may be studied not only with the use of the QCM technique, but also in the dynamical mode of an AFM. It is necessary to determine the dependencies of dynamical friction forces on the velocity, temperature, probe radius and its distance from the surface, the applied load, the dielectric properties of materials, the chemical composition and structure of a surface, the humidity (composition of surrounding atmosphere) and so on. In connection with the QCM technique and determination of the mechanisms of dynamical friction, it makes sense to study the z-dependences of the damping time of adsorbed films using adsorbed layers with different dimensions and types of molecules.

There is a need for more intensive studies of tribochemical, triboelectromagnetic and triboacoustic effects. In particular, the investigation of the sensitivity of normal and lateral forces to the chemical contrast is of great interest. Comprehensive information on the structure and properties of contacts can be obtained from measurements of the triboemission of particles on the nanostructural level.

4. Theory of friction forces in nanotribocontacts

4.1. Contact-mechanics approximations and comparison with AFM data.

Although the basic contact-mechanics approximations were developed for the description of macrocontacts [12 27, 73], in many cases these approximations allow one to obtain realistic estimates of some values measured with the use of an AFM on the atomic level, as was shown in a number of recent works [3, 32, 35]. Therefore, before proceeding to experimental data, we will briefly review basic theoretical relationships.

All the models considered describe an elastic contact of two convex bodies with radii of curvature of $R_{1,2}$. The oldest known version of the theory is the Hertz model which does not take account of adhesive forces. The Johnson – Kendall – Roberts model allows for adhesion in the contact approximation through incorporation of the adhesion work γ [see Eqn. (3.1)]. The Deryagin – Muller – Toporov approximation [27] takes into account not only adhesive forces themselves, but also their finite radius of action through the parameter z_0 corresponding to an equilibrium distance between two plane surfaces. In this case the shape of the contact area remains identical to that for the Hertz model and, in addition, the DMT theory adequately describes the contact of stiff surfaces with long-range attractive forces. The JKR model describes a contact of two surfaces made from soft materials and/or with large radii of curvature.

In the case when the interaction between the atoms of the bodies is given by the Lennard-Jones potential, the relationship between different versions of the theory is determined by the universal dimensionless parameter

$$\mu = 2.92\left(\frac{\gamma^2 R}{\widetilde{E}'^2 z_0^3}\right)^{1/3}, \tag{4.1}$$

where E' is the reduced modulus of elasticity [see Eqn (3.3)], and $R = R_1R_2/(R_1 + R_2)$ is the reduced radius of curvature. The 'Hertz' type solution is realized at $\mu = 0$; for $\mu < 1$ (actually for $\mu < 0.5$) the DMT limit holds, and $\mu > 1$ corresponds to the JKR limit.

For the intermediate case (at $\mu \approx 1$), the theory was generalized by Maugis and Dagdail (M – D) [104]. Recently, Barthel examined the case of an arbitrary form of the interaction potential (see the second reference in Ref. [105]).

For nanotribology, of prime importance are formulas for the radius of the contact area a and the adhesive friction force F determined by the second term in expression (2.5). These formulas can be written in the following approximations:

a) The Hertz approximation

$$a = \left(\frac{0.75RP}{E'}\right)^{1/3}, \tag{4.2a}$$

$$F = \pi\tau a^2; \tag{4.2b}$$

b) The JKR approximation

$$a = \left(\frac{9\pi\gamma R^2}{8E'}\right)^{1/3}\left(1 + \sqrt{1 + \frac{2P}{3\pi\gamma R}}\right)^{1/3}, \tag{4.3a}$$

$$F = \pi\tau a^2, \tag{4.3б}$$

and the critical force of probe detachment is determined by expression (3.3);

c) The DMT-approximation, in which a is determined by formula (4.2a) and the friction force is

$$F = \pi\tau\left(\frac{0.75R}{E'}\right)^{2/3}(-2\pi R\gamma + P)^{2/3}, \qquad (4.4)$$

and the critical force of detachment is obviously equal to $P_0 = -2\pi R\gamma$.

In all the formulas presented above τ is the shearing stress as before. In the M–D approximation the friction force is determined by formula (4.3b) with an additional multiplier (> 1) being obtained from a transcendental equation [104]. As follows from formulas (4.3a) and (4.3b), at the point of detachment of the probe from the surface the radius of the contact area and, correspondingly, the minimum value of the friction force remain finite [see Eqn (3.3)]. This is also true for the M–D approximation. In the case of the DMT approximation, at the point of probe detachment the friction force and the radius of the contact are zero. Thus, there is no hysteresis of the corresponding quantities.

Direct proportionality between the friction force and the area of the contact is observed both in AFM and SFA experiments. In experiments with the use of an SFA (for more details, see Ref. [3]), a linear pressure dependence of the shearing stress was found in the case of an LB film sandwiched between mica plates:

$$\tau = \tau_0 + \frac{\alpha P}{\pi a^2}, \qquad (4.5)$$

where τ_0 and α are empirical parameters.

For 'dry' contacts, τ does not depend on P. This is supported by the results obtained in work [47], where the friction forces for a silicon nitride probe on the mica surface were measured. In this experiment the friction force (as a function of the load) was measured immediately following the measurement of the contact stiffness. Using expressions (4.3b) and (2.4), it is easy to obtain the following formula for the shearing stress:

$$\tau = \frac{64G'^2F}{\pi k_c^2}, \qquad (4.6)$$

where k_c is the contact stiffness. As it turned out [47], the friction force F, the contact stiffness and, in accordance with formula (4.6), the shearing stress did not depend on the load, with the exception of the region of detachment of the probe from the surface where the effect of capillary forces manifested itself because of the presence of humidity (55%).

It follows from formulas (4.2)–(4.4) that the load dependence of the friction force is determined by two experimentally measured parameters: critical values of the detachment force and the friction force or, which is the same, any pair of values (P, F) on the $F(P)$ curve. In the case of an additional dependence between τ and y (see Section 3.2), the only indeterminate parameter of the model is the value of the reduced modulus of elasticity E' or the probe radius R. This makes it possible to use the AFM for determination of the mechanical, geometrical and adhesive characteristics of contacts.

The results of the best known experiments, where the $F(P)$ dependences for elastic nanocontacts in vacuum were measured, are presented in works [35, 43, 72]. To interpret the data obtained, the authors used the following approximations: DMT — in the case of a tungsten carbide probe on a (111) diamond surface [72] (this is the case of the stiffest contact, see Fig. 10); M–D — for the silicon–$NbSe_2$ contact [35]; JKR — for the Pt–mica contact [43] (Fig. 11). Some measured and calculated values relating to these experiments are listed in Table 1.

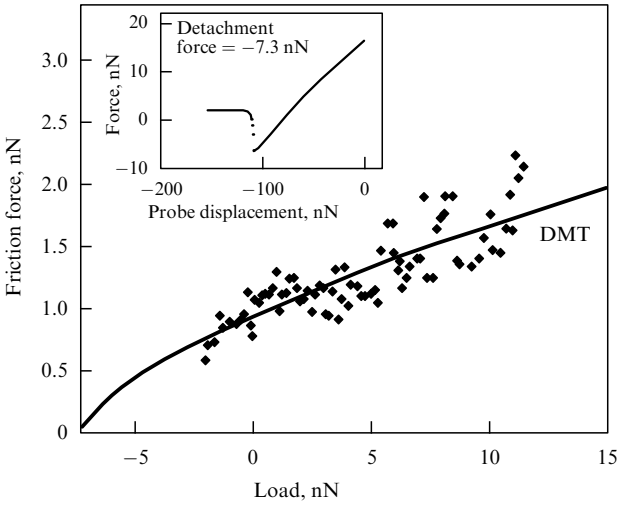

Figure 10. Experimental and theoretical (corresponding to the DMT model) dependence of the friction force on the loading force for a very stiff contact between a tungsten carbide probe and a (111) diamond surface treated by hydrogen. Inset: force-distance curve. The experimental value of the detachment force (−7.3 nN) correlates very well with the theoretical value predicted by the DMT curve. (Reproduced with the permission of Salmeron [72], copyright of the American Physical Society, 1998.)

Table 1. Empirical parameters measured with the use of AFMs in the case of 'dry' elastic nanotribocontacts in vacuum. Pairs of numbers in the last column correspond to maximum and minimum experimental values obtained in the process of friction scanning. (Reproduced with the permission of Salmeron [72], copyright of the American Physical Society, 1998.)

Work	[72]	[35]		[43]	
Model	DMT	M–D		JKR	
System	WC–diamond (111)	Si–$NbSe_2$		Pt–mica	
E', GPa	460.1	40.3		44.8	
z_0, nm	0.2	0.2		0.2	
R, nm	110	12	45	140	
F_0, nN	0	2.5	8.0	210	7.9
$-P_0$, nN	7.3	7.0	21.9	267	12
τ, GPa	0.238	0.61	0.66	0.921	0.27
γ, J m^{-2}	0.0106	0.099	0.087	0.404	0.019
μ	0.0065	0.61	0.58	0.38	0.07

Analysis of the above data shows that only experiments [35, 72] satisfy the conditions for applicability of the corresponding approximations (M–D and DMT) relative to the value of the μ parameter. Strictly speaking, in work [43] the μ value corresponds to the DMT or M–D approxima-

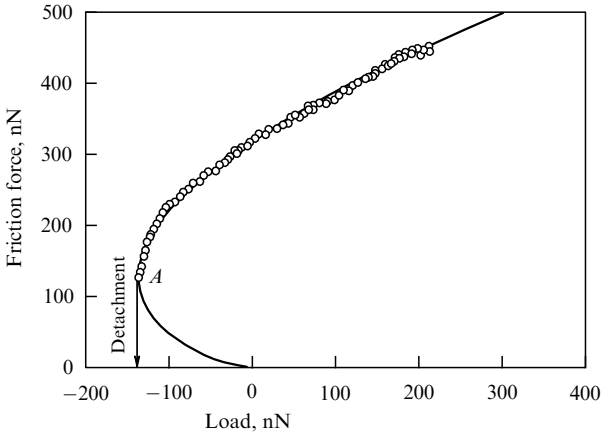

Figure 11. Characteristic 'friction force – loading force' curve for a platinum coated probe on a newly-cleaved mica surface in vacuum during a single scan along a given direction (see also Fig. 5). On the horizontal axis the external loading force (which is proportional to the vertical displacement of the cantilever) is plotted. The zeroth point corresponds to the off-contact position of the probe. On the vertical axis are the averaged critical values of the lateral forces for each value of the loading force (see Fig. 3). Note the nonlinear dependence of the friction force on the load and a finite value of the friction force at the point of detachment of the probe (A). The solid curve is plotted in accordance with the JKR approximation using the values of the friction force and the detachment force at the critical point of the contact. The lower part of the theoretical curve corresponds to unstable conditions, since the contact disappears at point A. (Reproduced with the permission of Salmeron [43], copyright of the American Physical Society, 1998.)

tions, however, the form of the experimental curves $F(P)$ is not described by these models and fits the JKR model. The authors believe that the monotonic decrease of the detachment forces and the critical friction forces for successive scan cycles is related to possible changes of the phase interface, and structural and chemical effects.

One important detail should be noted concerning experiment [72], namely, the very small calculated value of the shearing stress (0.238 GPa), even though the corresponding contact is the stiffest among all the contacts discussed.

If relationships between the macro- and microscopic values of physical quantities remain about the same, then it should be expected that the corresponding value of τ must be, as a minimum, an order larger. In this respect the results of work [35] show better agreement. Indeed, the measured value of τ and the macroscopic formula $G \approx 29\tau$ give an estimate for the shearing stress in good agreement with its macroscopic value.

It is possible that the underestimate of the shearing stress results from the illegality of extrapolation of the DMT dependence to the region of zero friction forces (see Fig. 10). However, in the experiment under discussion at the critical force of detachment (-7.3 nN) the friction force was not determined and its minimum value was measured only at a normal force of -2 nN. Thus, it is possible that, even though the DMT approximation correctly describes the $F(P)$ dependence in the range of loads from -2 to 12 nN, the minimum friction force in contrast with the theoretical prediction does not actually reduce to zero. In this case, to test the validity of the model, it is necessary to measure the $F(P)$ dependence for $P < -2$ nN using softer cantilevers.

Another subject for discussion concerns the interpretation of the results of work [43]. Despite the fact that the JKR approximation provides good agreement with the experimental $F(P)$ dependences, the value of the μ parameter seems too small for this model to be considered as being adequate to experimental conditions. In this connection doubts are cast upon the correctness of using formulas (3.2), (3.3) and hence the correctness of the above-mentioned relation $\tau \propto \gamma^{0.44}$ (see Section 3.2).

The results of work [35] reveal an interesting detail as well: as follows from Table 1, the adhesion work decreases with decreasing the radius of the probe, whereas the shearing stress, on the contrary, increases. Thus, we see that τ is inversely proportional to γ. None of the existing theoretical models can explain this result.

The above discussion shows that even in the simplest case of 'dry' elastic nanocontacts, the classical adhesive friction models may come into conflict with experiment. Such contradictions may be determined by experimental errors and/or by the influence of the atomic structure of surfaces and other effects which are ignored by the contact theory.

Linear $F(P)$ dependences which look nothing like those described by the contact-mechanics approximations were observed in experiments with alkaline-haloid crystals [71], GeS (Shwarz et al., [88]), LB and Au films, polytetrafluoroethylene (PTFE) films (PTFE is a polymeric lubricating material) as well as with multilayer structures based on PTFE and silicon nitride (Xin-Chun Lu, [88]). In the case of KCl and KBr crystals, these dependences are shown in Fig. 7. There is no theoretical explanation for these curves.

4.2 Simple models of friction forces, the stick-slip effect and modelling surface images in the contact AFM mode

The mechanical model of lateral movement of the probe over a surface is based on early work by Tomlinson [61] and the independent oscillator approximation. This model is schematically illustrated in Fig. 12 taken from the work by Zworner et al. [56]. A probe is elastically attached to a body of mass M connected to a cantilever via a spring of stiffness c. It interacts with the sample through a periodical potential $U(x)$, where x is the lateral coordinate of the probe. The cantilever moves with a constant velocity V_M. Independently of concrete microscopic mechanisms, the energy dissipation per unit

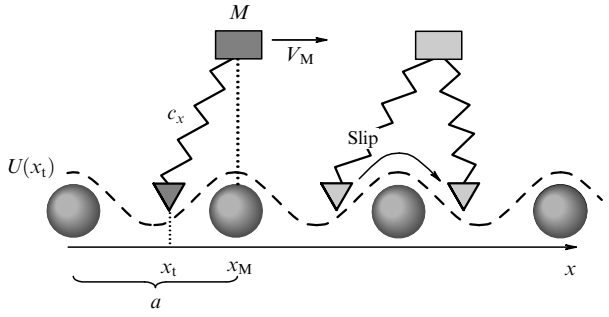

Figure 12. On the left: a simple model of probe slip along an atomically smooth surface; x_t is the lateral coordinate of the probe elastically attached to a body of mass M through a spring of stiffness c_x. Interaction with the surface is effected through a periodical potential $U(x_t)$ having a period a. At $x_t = x_M$ the spring is unstrained. When slipping, the body M moves with a velocity V_M in the x direction. On the right: the movement of the probe in a surface potential. If condition (4.8) is fulfilled, the movement is of a stick-slip character, and the probe 'jumps' from one point (of the minimum of the potential energy) to another. (Reproduced with the permission of Holscher [56], copyright of Springer-Verlag, 1982).

time is determined by the damping factor proportional to the velocity, whereas the friction force is independent of the velocity.

Obviously the point probe model gives an oversimplified description of the contact which is actually formed from several hundreds or thousands of atoms. In more complex models of friction, the region of the contact area is considered as an aggregate of a finite number of bound (not bound) oscillators. Despite their simplicity, models of this type quite successfully explain the spasmodic movement of a probe and allow one to model AFM images in the contact lateral mode [106].

Using the sinusoidal approximation for the periodical force acting between the probe and the surface, the equation for probe movement in the one-dimensional case can be written in the form [56]:

$$m\frac{\mathrm{d}^2x}{\mathrm{d}t^2} = c(x_\mathrm{M} - x) - U_0\frac{2\pi}{a}\sin\left(\frac{2\pi}{a}x\right) - \gamma\frac{\mathrm{d}x}{\mathrm{d}t}\,, \qquad (4.7)$$

where m is the effective mass of the oscillator, $x_\mathrm{M} = V_\mathrm{M}t$ is the equilibrium position of the unstrained spring at a moment t, and a and γ are the lattice period and the damping parameter, respectively. Solving equation (4.7) for $x(t)$, one can obtain the value of the lateral force acting on the probe: $F = c(x_\mathrm{M} - x)$. The dissipative friction force is determined by averaging the lateral force over time, $F_\mathrm{d} = \langle F\rangle$. If $V_\mathrm{M} = 0$ and the probe is in the state of stable equilibrium, then a critical condition for the start of the spasmodic movement of the probe is a small value of the stiffness of the cantilever compared to the lateral stiffness of the contact:

$$c < -\frac{\mathrm{d}^2U}{\mathrm{d}x^2} = \frac{4\pi^2U_0}{a^2}\,. \qquad (4.8)$$

In such a model, friction occurs only as the result of movement and is velocity-independent. For high velocities, 'viscous' damping dominates and the friction force is proportional to the slip velocity, $F_\mathrm{d} \approx \gamma V_\mathrm{M}$.

In the case of two-dimensional movement of the probe, equation (4.7) is generalized through incorporation of two effective masses, stiffnesses and damping parameters corresponding to the x and y directions [57].

In the case of high-oriented pyrolitic graphite (HOPG) being a test material for AFM, the potential of the interaction of the probe with a surface is approximated by the following model expression:

$$U_\mathrm{HOPG}(x,y) = -U_0\left[2\cos\left(\frac{2\pi}{a}x\right)\cos\left(\frac{2\pi}{a\sqrt{3}}y\right) + \cos\left(\frac{4\pi}{a\sqrt{3}}y\right)\right], \qquad (4.9)$$

where $a = 0.246$ nm, $U_0 = 0.5$ eV. Fig. 13 shows the experimental and calculated (computer simulated) distributions of lateral forces acting on an AFM probe on an HOPG surface [57]. The structure of the calculated force distributions is explained by the peculiarities of probe movement in the SS mode (Fig. 14). This figure shows that the probe moves spasmodically and is held back longest at the points of the minima of the potential corresponding to the centres of hexagons in the graphite lattice, 'jumping' over its maxima which correspond to the positions of carbon atoms. Fig. 14a also gives an explanation of the displacement of some points of the probe which 'stick' to the surface relative to the minima of the potential. Physically, this derives from the fact that after each microslip the probe cannot stop at once and under its own momentum 'rushes by' the point of equilibrium.

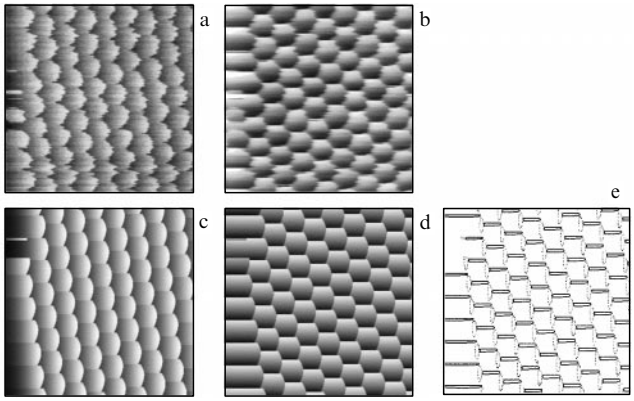

Figure 13. Comparison of experimental and calculated force distributions (scan area 2 nm × 2 nm); (a) and (b) correspond to the experimental data obtained with the use of an AFM on a newly-cleaved surface of HOPG. The experimental lateral-force distributions in the scan direction F_x (a) and transverse to this direction F_y (b) correspond to work [63]. Theoretical force distributions corresponding to the model described in the text are given for F_x (c) and F_y (d). A comparison between the figures shows that modelling even reproduces structural irregularities at the instant of the slip start (at the left of the images). The distances between individual maxima (0.246 nm) are the same on both the experimental and theoretical images. The scan direction makes an angle of 7° with the $[\bar{1}2\bar{1}0]$ axis of the (0001) graphite surface. (e) The maxima of the theoretical force distributions are indicated by points for the F_x projection and by solid lines for the F_y projection. A shift between them is seen. A similar phase shift between lateral forces in the scan direction and transverse to it was first observed by Ruan and Bhushan. (Reproduced with the permission of Holscher [57], copyright of the American Physical Society, 1998.)

The effective masses and stiffnesses of springs in the cited works satisfy the condition for critical damping: $\gamma = 2\sqrt{cm}$. Without this assumption the lattice periodicity of the SS effect fails and an irregular slip with multiple 'jumps' is observed.

It follows from calculations that the dissipative friction forces do not depend on the slip velocity for $V < 10^{-2}$ cm s^{-1}. At high velocities, viscous friction begins to dominate. This is in good agreement with the experimental measurements of the friction forces on diamond, graphite and amorphous carbon films [56]. True, the velocities studied in these experiments ranged from $2 \times 10^{-4} < V < 2.5 \times 10^{-3}$ cm s^{-1}. There is no question that such experiments should be carried out over a wider range.

In recent work [65] Johnson and Woodhouse generalized this model through incorporation of an additional stiffness of the contact k_e, since the assumption of critical damping of an elastic cantilever is unrealistic. The equivalent one-dimensional dynamical system considered in this work is shown in Fig. 15a and the corresponding dynamical equation takes the form [65]:

$$m\frac{\mathrm{d}^2x}{\mathrm{d}t^2} + \gamma\frac{\mathrm{d}x}{\mathrm{d}t} = T_0\sin\left(\frac{2\pi}{a}s\right) - k_lx\,, \qquad (4.10)$$

where $s = V_\mathrm{M}t - x - z$ is the tangential microslip of a sample relative to a probe. According to Fig. 15b, the value of the

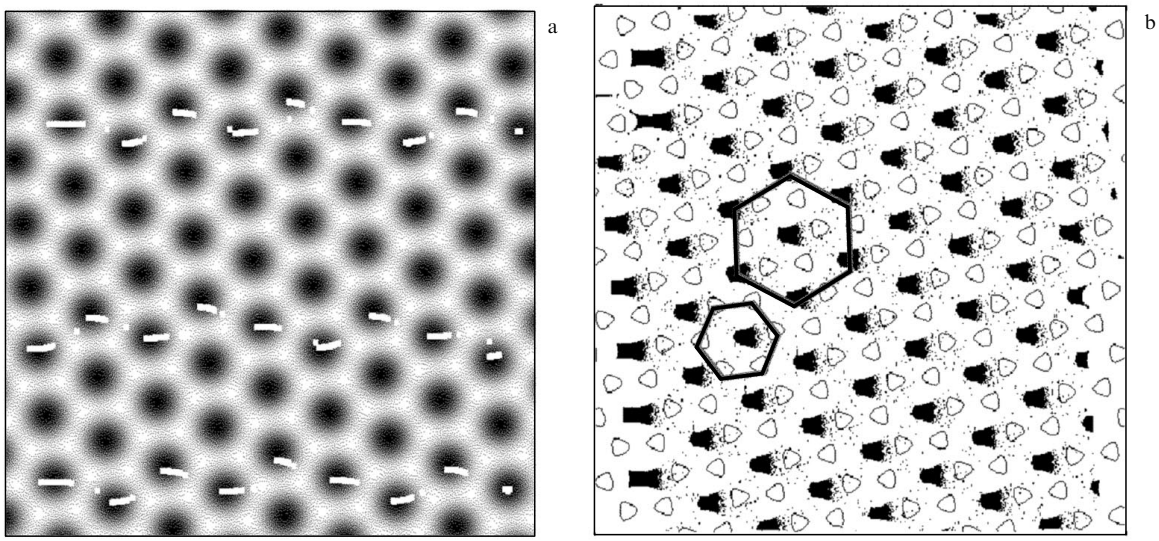

Figure 14. Two-dimensional distribution of the potential $U(x_t, y_t)$ on a surface of graphite (scan area 2 nm × 2 nm) and a typical calculated trajectory of probe slip along the surface. The time separation between the portions of the dotted line is $\Delta t = 0.1$ ms, the scan velocity is equal to $V_M = 40\ \text{nm s}^{-1}$. The figure confirms the two-dimensional character of the stick-slip effect: the probe moves with a discrete step and most of time stays at the positions of the minima of the surface potential (dark areas) (a). The light triangles show the *A* and *B* positions of carbon atoms with and without neighbours on the next nearest atomic plane in the lattice structure of graphite; these positions form hexagons (typical for the graphite structure) with a side length of about 0.142 nm. The dark spots characterize the rest time of the probe at the corresponding points of the surface (time resolution 512 × 512 dots). As is seen from this figure, the probe is held back longest at the centres of the hexagons. Hence the movement of the tip of an AFM probes the points of minima of the surface potential. Measurements of the lateral force contrast visualize the rhombic structure with a period of 0.246 nm [57] corresponding to the contrast of the minima of the potential rather than an 'atomic' contrast (b). (Reproduced with the permission of Holscher [57], copyright of the American Physical Society, 1998.)

microslip is

$$s = V_M t - x - \frac{1}{k_c} T_0 \sin\left(\frac{2\pi}{a} s\right). \tag{4.11}$$

In the quasi-static case (at $\mathrm{d}x/\mathrm{d}t = \mathrm{d}^2x/\mathrm{d}t^2 = 0$) x is obtained from Eqn (4.10) and Eqn (4.11) takes the form

$$\begin{aligned} s &= V_M t - \left(\frac{1}{k_c} + \frac{1}{k_l}\right) T_0 \sin\left(\frac{2\pi}{a} s\right) \\ &= V_M t - \frac{1}{k_e} T_0 \sin\left(\frac{2\pi}{a} s\right). \end{aligned} \tag{4.12}$$

On introducing new variables

$$S = \frac{s}{a}, \quad X = \frac{x}{a}, \quad Y = V_M \frac{t}{a}, \quad Z = \frac{z}{a},$$

$$K_c = \frac{a k_c}{T_0}, \quad K_l = \frac{a k_l}{T_0}, \quad q = \omega_l t, \quad \delta = \frac{\gamma \omega_l}{2k_l} \left(\omega_l = \sqrt{\frac{k_l}{m}}\right)$$

equations (4.10) and (4.11) are brought into normalized form

$$F_c(S) = \sin(2\pi S) = K_l\left(\frac{\mathrm{d}^2 X}{\mathrm{d}q^2} + 2\delta \frac{\mathrm{d}X}{\mathrm{d}q} + X\right), \tag{4.13}$$

$$S = Y - X - \frac{1}{K_c} \sin(2\pi S). \tag{4.14}$$

Figure 15c shows schematically the resulting change of the lateral force $F_c(S) = \sin(2\pi S)$ obtained from the numerical solutions of equations (4.13) and (4.14) and Fig. 15d its dependence on the displacement of the probe.

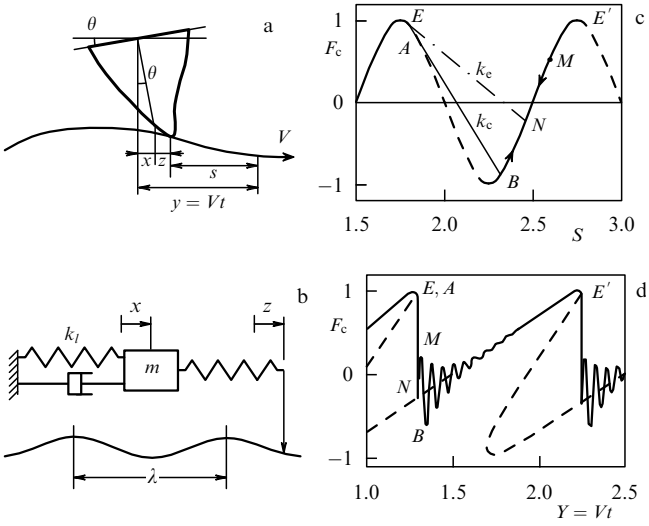

Figure 15. Lateral AFM mode. The torsion deflection of the cantilever through an angle θ results in a lateral displacement x; z is the contact displacement; s is the value of slip (a). Equivalent dynamical system: k_l and m represent the stiffness and equivalent mass of the cantilever, k_c is the contact stiffness (b). Sinusoidal change of the friction force F_c. The contact spring loses its stability at point *E* and then executes transition oscillatory motion about the position of equilibrium. The start of this motion corresponds to point *N* with a maximum deflection to point *M* (c). Dependence of the lateral force on the displacement Y reflecting a sawtooth character of the stick – slip effect (d). (Reproduced with the permission of K Johnson [65], the copyright of J C Baltzer AG, 1998.)

Segment *OE* corresponds to the stable quasi-static position of the probe. At point *E* an instability occurs and the cantilever begins to move in accordance with Eqn (4.13).

At $F_c(S) = -K_c$, the contact spring loses its stability and the probe 'jumps over' to point B. Because of the small mass of the spring, the corresponding relaxation time is of the order of 10^{-12} s that is much less than the period of the cantilever oscillation. Therefore, the elastic energy rapidly dissipates via phonon and electron excitations. Besides, $X_B = X_A$, $dX_A/dt = dX_B/dt \approx 0$, and the deformation of the contact spring is equal to $F_c(S)/K_c$. If the deflection of the oscillator at point M allows it to reach the point of instability E' corresponding to the next cycle of microslip, then before stopping the probe 'rushes by' two or more periods. There are no multiple jumps, if $S_M < S_{E_1}$. Thus, necessary conditions for this are $K_c > 2\pi$, $K_l > 1.9$. In any case there are no jumps, if $K_l > 0.75K_c$ [65].

The dissipative friction force can be calculated on the stable segment of the 'force–displacement' curve. Using a dimensionless analog of Eqn (4.12), we obtain

$$\begin{aligned}\langle F_f \rangle &= \int_{S_N}^{S_E} \sin(2\pi S)\left[1 + \frac{2\pi}{K_e}\cos(2\pi S)\right] dS \\ &= -\frac{1}{2\pi}\left[\cos(2\pi S_E) - \cos(2\pi S_N)\right] \\ &\quad - \frac{1}{4K_e}\left[\cos(4\pi S_E) - \cos(4\pi S_N)\right]. \end{aligned} \tag{4.15}$$

In accordance with Eqn (4.15), the dimensionless dissipative friction force decreases from 1 as $K_e \to 0$ to 0 for $K_e > 2\pi$ when the whole cycle of movement is stable. The same conclusion follows from the analysis of the K_c and K_l dependences of the friction force (see Figs 5a,b in work [65]).

Thus, the friction force decreases on increasing the contact and cantilever stiffnesses. However, this result is in contradiction with the experimentally stated relation $F_f \propto k_c^2$ for the contact of a silicon nitride probe and mica obtained in work [47] (see Section 4.1). Other experiments also show that the friction force increases with increasing contact stiffness. As was noted by the authors of work [65], it is possible that the lateral force has a constant component in addition to the sinusoidal fluctuating component. In any case, this aspect of the problem remains unclear.

Kerssemakers and De Hosson in a number of works [48] proposed a phenomenological (geometric) theory of the SS effect. They introduced a so-called critical displacement amplitude ('stick parameter') of the form $\varepsilon_0 = F_{max}/k_c(\alpha)$, where $k_c(\alpha)$ is the anisotropic lateral stiffness of the cantilever, and F_{max} is the maximum elastic force at the instant of the start of slip having a period λ. In moving the probe over hexagonal layered structures of $NbSe_2$ type, the region of lateral slip is bound by a circle of radius ε_0 and can be divided into six areas which characterize the directions of probable microslips corresponding to the strongest relaxation. Ultimately the path of the probe consists of a series of deformational-relaxational displacements taking place within the circle ε_0. Based on this model the authors of Refs [48] connected the observed spasmodic movement of the probe with contact anisotropy and expressed the quantity ε_0 in terms of the derivatives of the surface potential:

$$\varepsilon_0 = \frac{U'(\varepsilon_0)}{U''(\varepsilon_0)}.$$

Using the lateral modulation mode and this expression one can study the nonlinear characteristics of a tribocontact which are dependent on the form of the phase-interface potential relief. In the latest works [48], 'incomplete' microslips proving the existence of a lower threshold of occurrence of the SS effect were also observed.

4.3 Using the molecular dynamics method

Some results relating to the application of the MD method have already been considered in Section 3. Below we would like, first, to analyze in more detail the evolution of the atomic structure of the 'probe–surface' contact which can be visualized in numerical simulation experiments and, second, to consider the mechanisms of energy dissipation in the process of probe slip over a surface accompanied by variations of normal and lateral forces.

In representative computer simulation experiments [69, 82–84, 94] giving an insight into the atomic structure of nanocontacts, two types of probe movement are considered: along the normal to the surface of a sample (approaching and moving away) and lateral slip at a constant value of the normal force (or probe height). The upper layers of probe atoms are assumed to be stiff and are displaced in the normal or lateral direction with a step of the order of 0.005 nm. The sample is modelled by a finite set of parallel atomic planes (typically 10–20 planes) bound in the lateral plane by stiff walls; the lower surface is also assumed to be stiff. In the case of 'sharp' probes, the total number of atoms is 10–100, and in the case of 'blunt' probes, it is about 1000. The number of surface atoms ranges from 100 to 10000. One-dimensional models are also considered. Following each step of loading the contact along the normal or following lateral slip, the dynamical relaxation of the coordinates and the velocities of the atoms of the sample and the probe is performed for some time on the expiry of which the system may be considered as being in equilibrium, and its temperature reduces to a fixed value (usually close to zero) by multiplying all velocities by a corrective factor.

Figures 16a, b, c show the different stages of loading (a, b) and unloading (c) obtained by simulation of the contact of a sharp Ni probe consisting of 10 planes with (111) orientation ending with a single atom near its apex and a Cu (110) surface [69]. The projections of the positions of probe and surface atoms at different instants of time are shown [side view (a, c), top view (b)]. Figures 16d, e show the dependences of the normal forces on the probe displacements d and u corresponding to loading (d) and unloading (e).

When loading the contact, the probe begins to move when the distance between the apex and the surface is 0.4 nm. The instant at the beginning of the first sharp decrease of the normal force (point J_1 in Fig. 16d) corresponds to landing a Ni atom located on the probe apex in the centre of a square formed by Cu atoms (panel *1* in Fig. 16b). At $d = 4.3$ nm, 4 atoms of the probe (an apex atom and three upper ones) land in similar positions forming a commensurable (with the surface) structure (panel *2* in Fig. 16b). The force of attraction of the probe to the surface $F_N(d)$ decreases quasi-linearly on increasing d from 0.43 nm to 0.57 nm. At $d \approx 0.58$ nm, atomic layers adjacent to the contact area become disordered with the result that one layer of probe atoms 'disappears' within the 'thickness' of the surface ('dipping' in it), and this is accompanied by a sharp decrease of the normal force (point J_2). The processes of atom exchange between the probe and the surface accompany each phase of increasing $F_N(d)$, however, not all the sharp jumps of the normal force are connected with dipping the atoms of the probe. As d is increased, the contact area gradually grows in sizes including

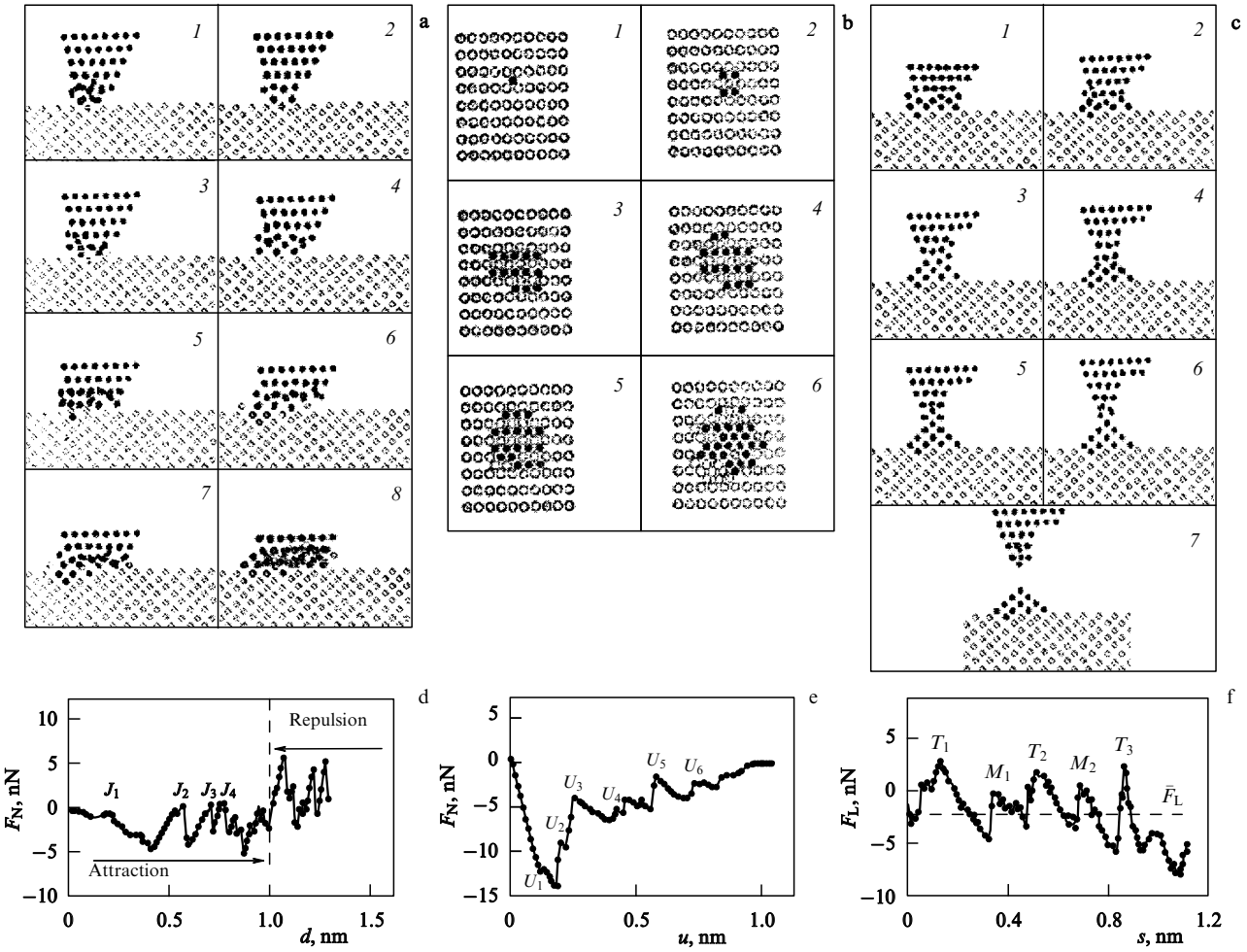

Figure 16. Atomic structure and forces in the tribocontact of a 'sharp' Ni(111) probe with a Cu(110) surface. The structure of the contact at indentation (loading), side view (a) and top view (b), as well as at unloading, side view (c), is shown. Panels in figures a-c corresponds to different phases of loading (unloading); at loading, panels *1–8* corresponds to displacements $d = 0.71$, 0.72, 0.8, 0.87, 1.11, 1.15, 1.22 and 1.29 nm, and at unloading, the start of unloading corresponds to $d = 1.01$ nm, and panels *1–7* correspond to displacements $u = 0.07$, 0.21, 0.42, 0.56, 0.63, 0.77 and 1.05 nm. The change of the normal (d, e) and lateral (f) forces on the contact as a function of the distance is shown. Nikel and copper atoms are indicated by solid and open circles, respectively. (From work [69]).

1, 4, 8, 13, 15, 18, 23, ... atoms. On the whole, for $0 < d < 1$ nm, the $F_N(d)$ force is attractive, exhibiting a multitude of small variations connected with the jumps of contacting atoms, since probe atoms, having a relatively small coordinating number, tend to decrease their energy forming a commensurate structure with the surface atoms. For $d > 1$ nm, the interaction of the probe with the sample as a whole takes on an attractive character, and the contact area begins to change its form (panels *5*, *6* in Fig. 16b).

The evolution of the contact area in the unloading condition when the probe moves up from the surface is shown in Fig. 16c. The start of the reverse movement corresponds to a depth of indentation $d = 1.01$ nm. The variation of the normal force with the displacement u is shown in Fig. 16e. The $F_N(u)$ dependence also demonstrates the presence of spasmodic variations (see points U_1, U_2, ...), however, they are not as regular as at the loading movement. The formation of new atomic layers in the contact area is accompanied by a sharp decrease of $F_N(u)$ at points U_1, U_2, ... In this case, before the formation of the layers, the structure of the contact bridge becomes disordered.

As was noted by many authors, the process of 'stretching' of the contact bridge and the formation of new atomic layers in this bridge is accompanied by 'order – disorder' type phase transitions affecting nanoscopic-scale regions. In the case being considered such a region counts for as few as several atoms in the cross section. At small u, the force $F_N(u)$ decreases with a large gradient, since the first structural change (point U_1) requires a considerable force. However, this point is intermediate, and only after transition U_2 may an originating atomic layer be identified. In periods of time between the formations of new layers, $F_N(u)$ increases quasi-linearly corresponding to a quasi-elastic deformation of the contact bridge. After transition U_5 the contact bridge makes up eight atomic layers under the surface. The disruption of the one-atom contact (at $u > 1$ nm) corresponds to an unloading force of about 1.5 nN. In the process of 'stretching' the contact bridge, the structure of the contact area adjacent to the surface is commensurable with the Cu(110) structure, and the structure of the upper layers of the probe becomes hexagonal and commensurable with the Ni(111) surface.

The variation of the lateral force $F_L(s)$ for probe displacement s is shown in Fig. 16f. In this case the normal loading force was 2.64 nN with a uniform distribution between the atoms of the upper atomic layers of the probe. The sharp jumps of $F_L(s)$ correspond to the SS effect with a

double period of about 0.35 nm being close to the lattice periods of Ni (0.352 nm) and Cu (0.361 nm). The points of structural transformations labelled T_i, $M_i\,(i = 1, 2, \ldots)$ follow each other in the course of each slip period, and the work needed to overcome $F_L(s)$ increases from one period to another. This seems to be connected with increasing the dimensions of the contact bridge, since, as follows from the results of computer simulation, after each slip phase the lower atomic layer of the probe is 'obliterated'.

The average value of the friction force in this numerical experiment was 2.06 nN. The process of probe movement is accompanied by transitions from an incommensurable (with the sample structure) structure of contacting layers to a commensurable one. These structural transformations occur during short periods of time. The slip generally starts at the interface between the Ni(111) and Ni(110) layers, where the last layer is commensurable with the Cu(110) structure. As was mentioned in Section 3.6, in metallic nanocontacts the variations of contact conductivity, being in synchrony with the variations of the normal force and the lateral force, are experimentally observed. Therefore the measurement of this conductivity can give valuable information on the atomic structure of contacts.

The authors of work [69] carried out a simulation of nanoindentation and slip friction for a model of a blunt Ni probe of hemispherical form involving 1580 atoms, that approximately corresponds to a radius of curvature of 4 nm, and Cu surface of 10 planes with (001) orientation involving 200 atoms (that is closer to the conditions of actual AFM experiments). The (001) orientation of the atomic layers of Ni is pseudomorphous to the Cu(001) structure. In the process of lateral slip of the probe, a normal loading force of 9.1 and 12.9 nN was applied to it. As follows from simulation results, the average lateral force applied to the probe over several stick – slip cycles (Fig. 17) was close to 14 nN (under a load of 9.1 nN).

As follows from comparison of this data (with consideration for the value of the detachment force: -25 nN) and the JKR contact model, which is applicable to this case, a satisfactory agreement with this model may be obtained at $\gamma = 1.3$ J m^{-2}, $\tau = 3.7$ GPa. Thus, the value of the adhesion work obtained is about twice as small as its macroscopic value for the contact of hard nickel with copper (about 2.8 J m^{-2}). However, the shearing stress seems to be overestimated, since in this case the shear modulus is equal to 17 GPa and, correspondingly, $G/\tau = 8.5$ rather than 29 (a characteristic value in macroconditions).

The structure of the contact area and the variation of the lateral force acting on the hemispherical Ni probe are shown in Fig. 17. Panels *1* and *2* correspond to normal forces of 9.1 nN and 12.9 nN, respectively. In the initial phase of probe slip (under a load of 9.1 nN), the lower layer of probe atoms involving 24 atoms is in contact with the surface. The corresponding contact area is relatively large and has a plane shape, therefore the character of slip differs from that considered in the case of a sharp probe. The SS effect now exhibits a periodicity of about 0.15 nm, and the structural changes of the T_i or M_i types observed in the case of a sharp probe are not resolved.

Under a load of 9.1 nN (panel *1*), the Ni surface 'sticks' to the Cu surface and the 'stiff' upper layers of the probe are displaced relative to the lower ones. Below the interface surface linear dislocations are seen. Panel *2* corresponds to the end of the slip phase. The structure of atomic layers

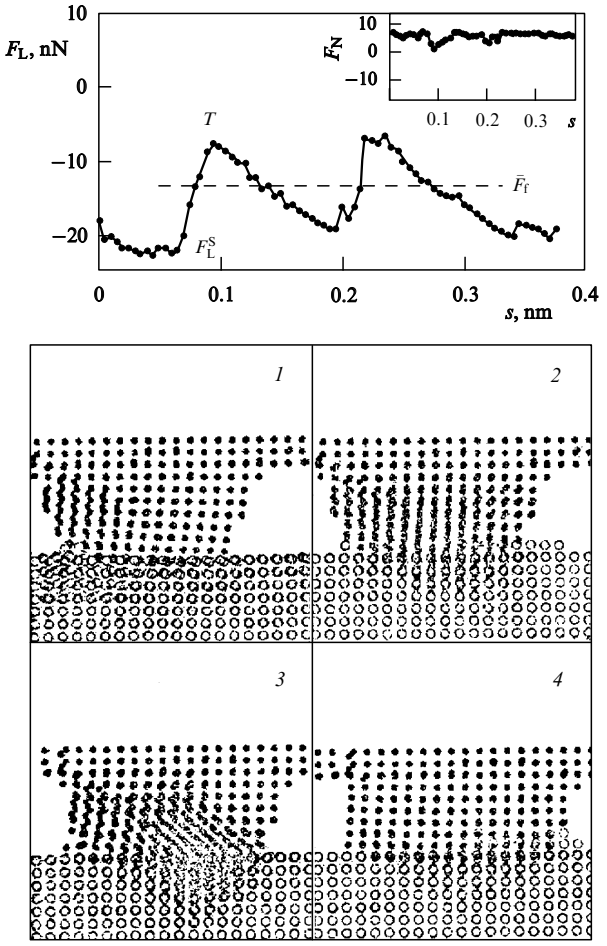

Figure 17. Atomic structure and forces in the tribocontact of a hemispherical nickel probe [1580 atoms, (011) orientation of layers] with a Cu(001) surface. Solid circles – Ni atoms, open circles – Cu atoms. (From work [69]).

becomes disordered, some atoms of nickel and copper exchange their sites, and the hemisphere shifts as a whole in the (100) direction. After completion of the slip phase, the structure of the atomic layers is restored once the atoms of Ni shift to their new equilibrium position. Panels *3*, *4* show similar contact structures (in the stick phase and after the slip phase) at a normal load of 12.9 nN. In this case the contact structures are more highly disordered, and the SS effect is less regular.

It is also seen from Fig. 17 that the ratio of the static friction force F_L^S to the average lateral force $\langle F_L \rangle$ is roughly 2. In AFM experiments (see Fig. 3) this ratio is close to 1.5.

In works [82] the authors in their simulation experiments define so-called 'internal' and 'external' friction forces in such a way that the first of them is connected with the increment of the total energy of a model tribosystem related to the length of an elementary microslip (at the successive steps of simulation) and the second is considered as the increment of a remanent (after performing dynamical relaxation) lateral force acting on the probe after each step. It is the author's opinion that such a definition of the friction forces does not adequately take into account their dissipative nature, since the corresponding contributions contain a high portion of conservative forces. Without

considering the kinetic energy of the atoms (in this definition), we must obtain near-zero friction forces, if a microslip corresponds to one lattice period of a surface structure. This follows from the identity of atom configurations, if the effects of atom mixing are not taken into account. The authors of works [82] actually believe that the kinetic energy of a probe is thermalized in a contact area involving a limited number of probe and surface atoms. In this case continuous local heating of the system takes place, whereas in the real situation the thermal energy must go out into the volumes of the contacting bodies. As to work [69], the authors do not take into account losses connected with heating the tribocontact, and the integration of the lateral force over the slip period may result in a contribution of conservative forces having nothing to do with friction.

Summing up the results of the last three sections, one can state that the numerical MD experiments allow one to create a realistic physical picture of the evolution of an atomic structure in the 'probe-surface' contact area for loading, unloading and the lateral movement of a probe, however, the problem of the practical calculation and prediction of the friction forces under the condition of AFM experiments still remain to be solved. Using the contact-mechanics approximation, one can (at least for elastic contacts) calculate the adhesive friction forces, but attempts to reflect correctly the role of the atomic structure do not meet with success. Moreover, the empirical parameters of the theory may be grossly changed when going to an atomic scale. As to the simple models considered in Section 4.2, they provide a convenient way of modelling surface images observed in AFM, but also do not allow one to obtain a detailed quantitative description of friction forces.

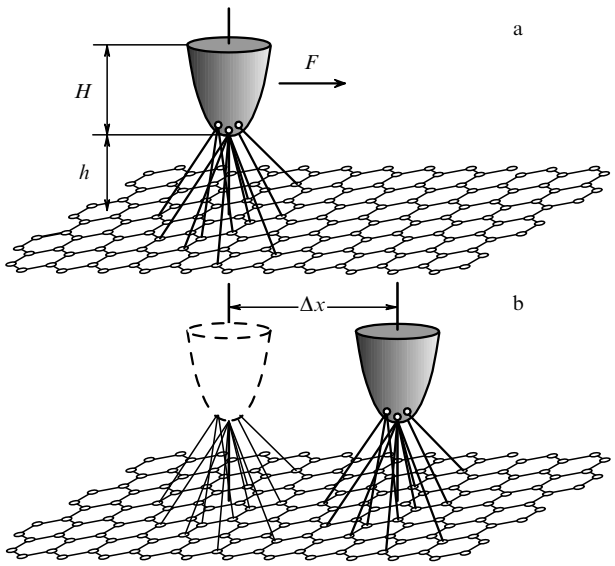

Figure 18. Mechanism of energy dissipation with adhesive friction. (a) Probe is located at a position corresponding to the minimum of the energy of the 'probe-surface' system. Solid lines show individual adhesive bonds between the atoms of the probe and the surface. The contact area is shown in a simplified form without considering deformation. The atoms of the surface making these adhesive bonds are at inequilibrium positions relative to those at distances well away from the contact area. (b) New equilibrium position of the probe after a sudden microslip over a surface structure period. 'Old' adhesive bonds have no time to relax. They are shown by thin lines, and newly formed bonds are shown by solid lines. Atoms on both of these bonds come to oscillatory motion, and their excess energy goes into heat via the phonon subsystem. The friction force is the ratio of the total bond-breaking energy to the displacement of the probe.

4.4 Theory of adhesive friction

The basic ideas of this theory were considered in work [75]. The corresponding mechanism is illustrated in Fig. 18. Initially the probe is located at a position corresponding to the minimum energy of a tribosystem. Individual lines connecting the atoms of the probe and the surface in Fig. 18a correspond to established adhesive bonds. If the lateral force applied to the probe exceeds the critical value of the friction force at rest, then a drastic microslip occurs, being catastrophic in character, and the probe is displaced over a distance Δx in the lateral direction. Since this displacement takes place in a very short time interval (probably about 10^{-12} s), the adhesive bonds have no time to relax and therefore, on the one hand, the abrupt breaking of old bonds, and on the other, the avalanche-like making of new bonds (corresponding to a finite position of the probe) occur (Fig. 18b). As a result the atoms of the surface and the probe come into oscillatory motion whose energy eventually transforms into heat. This argumentation is close to ideas argued in the work by Teibor [28]. The foundations of this theory can be concretized as follows:

a) the amount of energy dissipated into heat in one microslip is determined by the sum of the absolute changes of the energy of individual adhesive bonds (Δw_k corresponds to k-th adhesive pair):

$$\Delta W = \sum_k |\Delta w_k| \,; \tag{4.16}$$

b) an elementary microslip has a length of the order of the lattice period, $\Delta x = d$;

c) the friction force is equal to

$$F = \frac{\Delta W}{\Delta x} \,. \tag{4.17}$$

The first calculations in the framework of this scheme [75] were performed for a simplified case without considering the deformation of the contact area and the relaxation of the atomic structure. Silicon – silicon and W (probe) – (100) α-Fe contacts were considered. The dependence of the normal force applied to the contacts on the height h and the radius of the probe has a power form ($F \propto h^{-3.5}$) and a near-linear form, respectively, that is in good agreement with experimental results [35]. The calculated 'friction-load' curve is similar to that obtained in work [35] for Si – $NbSe_2$ contacts. In works [66] this model was generalized with consideration for the deformation of the contact area given by a model function. The parameters of this function were determined from the condition for the minimum of the tribosystem energy which includes the 'probe – sample' interaction and the deformation energy of the bonds for the sample. It is assumed that the probe is stiff and retains the atomic structure of the initial material. Fig. 19 shows the results of calculation of the dependences of the friction forces on the loading force and the radius of a parabolic probe for the 'diamond – graphite' system. The corresponding curves are plotted with (Fig. 19a) or without (Fig. 19b) considering the deformation of the contact area. It makes sense to compare these theoretical dependencies with the results of experiments [35, 43, 72], in which the 'friction force – loading force' curves were obtained for the following contacts: Si (probe) – $NbSe_2$

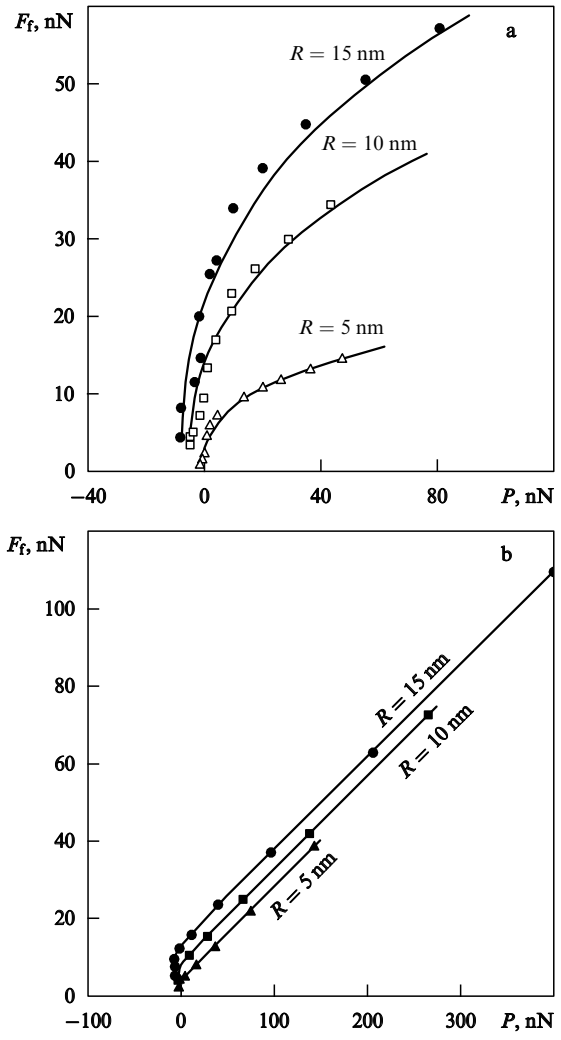

Figure 19. Model theoretical dependences of the adhesive friction force for a stiff diamond probe on the (0001) graphite surface on the loading force and the radius of the probe: with (a) and without (b) deformation of the contact area. Solid curves are plotted for the sake of convenience. (From work [66])

(the radii of curvature of the probes are 12 and 48 nm); diamond (probe)–tungsten carbide (with a radius of curvature of 110 nm) and Pt (probe)–mica (with a radius of curvature of 140 nm).

Correlating the dependencies presented in these works with Fig. 19a, one can note the same irregular character of experimental points at small loading forces. In this case the irregularities are more pronounced at small radii of the probe when the discreteness of the atomic structure manifests itself more clearly. It should be noted that without considering the deformation of the contact area, the theoretical 'friction-load' dependences are smooth and resemble the run of similar curves for the contact-mechanics models (see Fig.19). The results of calculation [66] at $R = 10$ nm and the data for Si–$NbSe_2$ [35] at $R = 12$ nm are in qualitative agreement, whereas in a quantitative sense the theoretical values of friction forces are two-three times larger. This distinction may be connected with the presence of different types of interacting atoms and, correspondingly, with the difference in the force characteristics of tribosystems as well as with the inaccuracy of formula (4.17) and/or experimental errors.

The conclusion that the friction force is proportional to the radius of curvature of the probe is supported by experimental data [35, 43]. Indeed, for the Pt–mica contact ($R = 140$ nm) [43] the friction forces are an order higher than those in the case of the Si–$NbSe_2$ contact ($R = 12$nm). As was mentioned in Section 4.1, in experiments [72] one obtained anomalously low values of friction forces at a large probe radius (110 nm) as well as too low (for such a stiff contact) a value of the shearing stress (238 MPa), calculated in the DMT approximation. It is likely that the radius of curvature of an outward-projecting part was about 10 nm.

As was mentioned at the end of Section 3.1, the adhesive model gives a qualitative picture of the atomic periodicity of the SS effect. The detailed quantitative calculations of lateral forces as well as the investigation of the energy threshold for occurrence of slip still remain to be done. The success of the phenomenological approach used in work [48] (See Section 3.1) also counts in favour of the key role of geometry in occurring the SS effect. The periodicity of normal forces and the inversion of normal force contrast depending on the ratio a/d (a is the radius of a nanowire) were obtained in calculations of the interaction of single and multilayer nanowires with a surface [53].

A theory outlined in work [75] leads to a new (macroscopic) relation between the shearing stress (the shear modulus) and the surface energy of solids (see Fig. 6). In the case of a plane contact of two bodies with an area A, the adhesion energy is $W = \gamma A$, where γ is the adhesion work determined by formula (3.2). In a sudden microslip over the distance d such energy goes into the breaking and making of new adhesive bonds, that is, dissipates into heat. Therefore the friction force is

$$F = \frac{\gamma A}{d} . \tag{4.18}$$

Taking into account formulas (4.18) and (2.5), we obtain for the adhesive friction force

$$\tau = \frac{\gamma}{d} . \tag{4.19}$$

For the contact of homogeneous materials, with consideration for expression (3.2) and relation $\gamma_{12} = 0$, formula (4.19) takes the form $\tau = 2\sigma/d$, where σ is the specific surface energy. In addition, by virtue of the proportionality between the macroscopic shear modulus G and the shearing stress τ, the last result can be transformed into an equivalent form $Gr \propto \sigma$, where $r = d/2$ is the atom radius. Figure 6 supports the conclusion that this correlation in fact holds.

4.5 Dynamical friction forces

When a probe moves with a velocity V over the surface of a sample, the energy of its onward movement can dissipate through dynamical mechanisms giving no contribution to the friction force in the static case. Among the most important mechanisms of this type are the fluctuation-electromagnetic interaction as well as the processes of excitations of electrons and phonons [8, 9]. We will differentiate fluctuation-electromagnetic and electron processes, assigning to the latter the effects which are determined by the short-range excitations of electron plasma and by the formation of electron-hole pairs, whereas the fluctuation-electromagnetic interaction will be considered as a long-range effect taking place in the case when a probe and a surface are separated by a vacuum interlayer. This viewpoint differs from the interpretation used in a recent

paper by Tomassone and Widom [107] who considered electron processes in a wider sense combining them with fluctuation-electromagnetic ones.

Without question a self-consistent quantum theory must take into account all possible types of excitations in a unified way, however, at the present time it is still in the initial stage of development. In any case the specification of individual mechanisms is essential for a more fundamental understanding.

It should be noted that a typical scan velocities in an AFM are much less than the sound velocity and the Fermi velocity of electrons, therefore, in the absence of damping of phonon and plasmon modes, the processes of one-particle excitations are forbidden by the law of conservation of energy–momentum. For example, the generation of single acoustic phonons by a moving atom (probe) is possible for $V > V_s$ (where V_s is the sound velocity). In this case phonons are emitted within the Cherenkov cone $\cos\theta = V_s/V$. With finite damping, particles may loss their energy by excitation of quasi-particles at arbitrarily small velocities.

As was mentioned in Section 4.4, elementary excitations always accompany the finite stages of tribosystem-energy dissipation in stick-slip processes, that is, in the contact mode of an AFM, but in this case we mean only dissipative (viscous) velocity-proportional forces acting between the probe and the surface which can be considered as relatively weak. Indeed, in the case of the contact mode, the total work performed by these forces (if we use an estimate on the basis of subsequent analysis) does not exceed 1 pH $\times 2 \times 10^{-10}$ m $= 2 \times 10^{-22}$ J, whereas the adhesive friction forces are three-four orders of magnitude larger. However, this estimate is based on an average value of the probe velocity of 1 m s $^{-1}$ and if a microslip takes place in a time of 10^{-12} s, this value should be increased by two orders of magnitude, and then the viscous force may be comparable with the static friction force. In any case dynamical friction has to play a large role in quartz crystal microbalance and SFA experiments and in the modulation mode of AFM.

Fluctuation-electromagnetic friction forces. Despite the simplicity of the main idea (a moving fluctuating dipole induces surface electrical currents, whose Joule damping is the final result of friction), so far, when calculating the corresponding forces, there is no clarity in respect to a number of main factors, such as the dependences of these forces on the velocity, distance, temperature and so on (see, for example, works [9, 108–112] and references in these works). It is the author's opinion that the most common approach to the solution of this problem is given by the Lifshitz fluctuation-electromagnetic theory, therefore we use below the results obtained in the framework of this theory [108–110].

Assuming that a neutral atom having a velocity V moves parallel to a surface on a distance z from it (z exceeds typical atomic sizes), for the lateral (friction) force acting on this atom (in the linear approximation with respect to the velocity) one can write

$$F = -\frac{3\hbar V}{8\pi z^5}\int_0^\infty \mathrm{d}\omega\left\{2\left[\alpha''(\omega)\frac{\mathrm{d}\Delta''(\omega)}{\mathrm{d}\omega} - \Delta''(\omega)\frac{\mathrm{d}\alpha''(\omega)}{\mathrm{d}\omega}\right] + \omega\left[\alpha''(\omega)\frac{\mathrm{d}^2\Delta''(\omega)}{\mathrm{d}\omega^2} - \Delta''(\omega)\frac{\mathrm{d}^2\alpha''(\omega)}{\mathrm{d}\omega^2}\right]\right\}\coth\left(\frac{\omega\hbar}{2k_\mathrm{B}T}\right), \tag{4.20}$$

where $\alpha(\omega)$ is the atomic polarizability, $\Delta(\omega) = [\varepsilon(\omega) - 1]/[\varepsilon(\omega) + 1]$, $\varepsilon(\omega)$ is the dielectric function of the medium, and k_B, $\hbar$ and T are the Boltzmann contact, Planck constant and the temperature, respectively. The quantities with two primes correspond to the imaginary parts of the corresponding functions. For the normal (to the surface) movement of a neutral particle, a formula similar to Eqn (4.20) is not available.

It follows from formula (4.20) that at $T = 0$ the friction force does not equal zero, which is a physical result of the existence of zero fluctuations of an electromagnetic field in the substance. At $T = 0$, formula (4.20) can be transformed into the simple-form used in work [75]:

$$F = -\frac{3\hbar V}{4\pi z^5}\int_0^\infty \mathrm{d}\omega\alpha''(\omega)\frac{\mathrm{d}\Delta''(\omega)}{\mathrm{d}\omega}\,. \tag{4.21}$$

Assume that the strongest line in the absorption spectrum of an atom has a frequency ω_0. Then, assuming the damping coefficient to be zero, for the imaginary part of polarizability we obtain

$$\alpha''(\omega) = \frac{\pi e^2 f_0}{2m\omega_0}\delta(\omega - \omega_0)\,, \tag{4.22}$$

where e, m, f_0 are the electron charge, the electron mass and the oscillator strength, respectively. Using the standard Lorentz–Drude model approximation for the dielectric function of metal and substituting Eqn (4.21) in Eqn (4.22), we obtain [110]

$$F = \frac{3\hbar e^2 f_0 \tau^2 V}{4mz^5}\frac{y^2(12x^4 - 4x^2y^2 + 4x^2 - y^4)}{x(4x^4 - 4x^2y^2 + 4x^2 + y^4)^2}\,, \tag{4.23}$$

where $x = \omega_0\tau$, $y = \omega_\mathrm{p}\tau$, ω_p and τ are the plasma frequency and the relaxation time of metal electrons, respectively. The analysis of formula (4.23) shows that the sign of F depends on the relation between the absorption frequency of an atom and the plasma frequency. The force is braking for $\omega_\mathrm{p} \geqslant \sqrt{2}\omega_0$. For metals, typical values of parameters τ and ω_p are about 10^{-14}–10^{-15}s and 5–10 eV, respectively. In this case the above condition is fulfilled, however, for the high-frequency lines of atomic absorption, the opposite situation is possible, and the lateral force may become accelerating. However, it should be noted that the absolute values of the spectra-overlap integral determined by the x, y-dependent factor in formula (4.23) decrease with increasing ω_0, therefore, to estimate correctly the total force F, it is necessary to take into account in detail the absorption spectrum of the atom in a narrow frequency region near $\omega_\mathrm{p}/\sqrt{2}$. Calculations show that for a typical QCM experiment [21, 22] in the case of adsorption of a krypton atom on gold, the value of the spectra-overlap integral, being determined by the x, y-dependent factor in formula (4.23), is close to -0.1. Then at $z = 0.04$ nm the motion damping time is $\Delta t = MV/F = 0.6$ ns (M is the mass of a krypton atom), which is close to the experimental value.

In the additive approximation [108, 109], the lateral friction force acting on a moving parabolic probe with a distance h between the apex and the surface can be obtained from formula (4.20). Expressing $\alpha(\omega)$ via the dielectric function of probe material $\varepsilon_1(\omega)$ with the use of the Clausius–Mossotti formula and integrating over the volume of the probe, we obtain

$$F = -\frac{3}{64\pi}\frac{\hbar R V}{h^3}J\big(\varepsilon_1(\omega), \varepsilon(\omega)\big)\,, \tag{4.24}$$

where R is the radius of curvature of the probe, and the frequency integral $J(\varepsilon_1(\omega), \varepsilon(\omega))$ coincides with that in formula (4.20) with replacing atomic polarizability by $\widetilde{\Delta}''(\omega) = \mathrm{Im}\{[\varepsilon_1(\omega) - 1]/[\varepsilon_1(\omega) + 2]\}$.

As follows from formula (4.24), the temperature dependence of the friction force becomes essential for $\omega\hbar \leqslant 2k_B T$, when $\coth x \to x^{-1}$. At room temperatures $2k_B T \approx 0.05$ eV, therefore, the processes of low-frequency absorption, such as dipole relaxation (in dielectrics) and infrared absorption in ionic and conducting crystals, contribute predominantly to the friction force.

The numerical estimates of the friction force from formula (4.24) performed for different combinations of materials show that for typical probes with $R = 10-20$ nm, at $V = 1$ m s^{-1}, $z = 0.2-0.3$ nm and at room temperatures the values obtained fall in the range 0.1 to 10 pN. Such forces can materially contribute to the damping coefficients of the lateral oscillation of AFM cantilevers, if these latter have Q of the order of $10^4 - 10^5$. The Q-value related to the dynamic friction force can be estimated with the use of the following formula: $Q = k_l V / 2\Omega_l F$, where k_l is the stiffness defined by formula (2.2) and the frequency Ω_l is likely to be an order higher than the normal-oscillation frequency [see expression (2.3)]. For stiffness 100 N m^{-1}, frequency $10^6 - 10^7$ Hz, velocity 1 m s^{-1} and force 1–10 pN, one obtains $Q = 5 \times 10^5 - 5 \times 10^7$, therefore, the measurement of the Q-shift resulting from an electromagnetic link between a probe and a surface is a real experimental task.

Electron friction. The mechanism of electron friction due to the generation of electron–hole pairs was first analyzed by Persson (see references in work [89]) in connection with the problem of damping the lateral oscillation of films adsorbed on a metallic substrate. An interrelation between the friction force resulting from the scattering of conduction electrons by oscillating adsorbate atoms and the change of resistance of a metal was used. Designate the inverse damping time of the lateral oscillation of an adsorbate atom as $1/\tau_A$, then the dynamic equation for conduction electrons will include an additional contribution to the friction force equal to $Mn_A V / mnd\tau_A$, where M is the mass of a surface atom and n_A is the surface density of atoms in a film, m, n and d are the mass of the film, the density of conduction electrons and the film thickness, respectively. The velocity-proportional coefficient can be considered as the inverse relaxation time due to an additional mechanism of electron scattering, $1/\tau_e$. As a result, resistivity is increased by a factor of $\Delta\rho = m/ne^2\tau_e = Mn_A/n^2e^2\tau_A$, and the required damping time τ_A is

$$\tau_A = \frac{Mn_A}{n^2e^2d\Delta\rho} \,. \tag{4.25}$$

This theory gives an adequate estimate of the lateral-motion damping time for molecules in the case of physical and chemical adsorption, however, it is too simple and does not take into account the structure of the film and the character of the electron distribution near the film surface.

In work [113], an expression for the braking losses of a hydrogen atom by excitation of the electrons of metal was obtained on the basis of the quantum perturbation theory. Conduction electrons were considered in the 'jelly' model with a sharp jump of potential at the boundary. On the assumption that for heavy atoms of mass M the braking force remains the same, one obtains the following formula for the lateral motion damping time:

$$\Delta t = \frac{MV}{F} = \frac{2\pi M}{27\hbar a_B^2 k_F^4} \,, \tag{4.26}$$

where k_F is the Fermi vector of the electrons of metal, a_B is the Bohr radius. Assuming that $k_F = 10^8$ cm^{-1} and $M = 1.4 \times 10^{-25}$ kg (krypton), one obtains $\Delta t = 1.1 \times 10^{-11}$ s. This value is two orders of magnitude less than experimental values. Two factors, however, must result in an additional decrease of Δt: first, for atoms with a large nuclear charge, the losses of energy must be larger, since the effective charge of heavy atoms is greater than unity; second, for films with a regular periodic structure, Δt decreases N times (N is the number of atoms in a film [114]). Thus, the theory being considered gives too large values for the electron friction force and small values for the motion damping time for adsorbed films.

Another approach to the problem of electron friction was proposed in work [75]. The corresponding mechanism is based on a phenomenological theory of braking losses of slow ions in solids (see references in work [75]): the losses of energy result from a hypothetic exchange of electrons belonging to a moving atom, on the one hand, and to an atom of the target, on the other (in the case of AFM, an exchange of atoms takes place between the probe and the surface). Each electron of the probe passing through the equipotential surface of the 'probe-surface' system loses the relative-movement momentum mV. In fact, this argumentation is close to the Persson model relating the braking force with the process of electron scattering. In accordance with this theory, the loss of energy of a neutral atom with nuclear charge Z_1 and velocity V flying at a sighting distance b from a surface atom with nuclear charge Z_2 is

$$\Delta E = -\frac{me^2}{\hbar} \frac{0.35(Z_1 + Z_2)^{5/3}}{\left[1 + 0.16(Z_1 + Z_2)^{1/3} b/a_B\right]^5} \, V \,. \tag{4.27}$$

Assuming that the sample has a uniform distribution of atoms with a density n and the moving atom is a distance z from the surface, upon integration of formula (4.27) over all possible sighting parameters, we find

$$\frac{dE}{dx} = F(z) = -0.7(Z_1 + Z_2)^{5/3} \frac{me^2}{\hbar} nV \times \int_z^\infty \frac{b \arccos(z/b)\, db}{\left[1 + 0.16(Z_1 + Z_2)^{1/3} b/a_B\right]^5} \,. \tag{4.28}$$

For a Kr atom on the gold surface formula (4.28) gives $F(z) = 1.7 \times 10^{-16} z^{-2.4} V$ nN (z is measured in angstroms, V in m s^{-1}), hence it follows that the damping time at $z = 0.35$ nm approximates 1ns, in good agreement with experiment.

From this theory one can also easily obtain a braking force acting on an AFM probe with the use of the 'jelly' model and the locally-plane approximation for the electron distribution within a uniform metallic contact formed by a parabolic probe with a radius of curvature R and a plane surface [75]:

$$F \approx -\frac{3\pi}{10} (3\pi^2)^{1/3} \hbar V n_e^{4/3} \frac{(R + h/2)^2}{b^2 R^2} (1 + bR) \exp(-bh) \,, \tag{4.29}$$

where h is the distance of the probe apex from the surface, and n_e is the electron density in metal. In the case of the Al – Al contact $b \approx 1.19\ \text{nm}^{-1}$, then at $R = 20$ nm, $h = 0.2$ nm, $V = 1$ m s^{-1} from formula (4.29) one obtains $F \approx 0.67$ pN. In the case of the contact of nonconducting bodies, the role of this mechanism is likely to be insignificant.

Phonon friction. There is also no commonly accepted viewpoint regarding dynamic phonon friction. This is connected to some extent with the fact that the corresponding mechanism manifests itself on the background of structural effects, whose role was mentioned above and which may be induced by the mechanism of the breaking of adhesive bonds.

Sokoloff, using the perturbation theory, obtained the following formula for the braking force of a single adsorbed atom in a film [114]:

$$F = \frac{1}{M}\sum_{\mathbf{k}} \frac{\gamma k_x^2 |f(\mathbf{k})|^2 V}{\left[\Omega_0(\mathbf{k})^2 - k_x^2 V^2\right]^2 + \gamma^2 k_x^2 V^2}\,, \tag{4.30}$$

where $\Omega_0(\mathbf{k})$ is the phonon frequency, γ is the inverse damping time, k_x is the projection of the phonon wave vector $\mathbf{k}$ onto the direction of movement, V and M are the velocity and mass of the atom, respectively, and $f(\mathbf{k})$ is the two-dimensional Fourier transform of the force of interaction with the surface. For a periodic force, $f(\mathbf{k})$ is proportional to $\delta_{\mathbf{k},\mathbf{G}}$, where $\mathbf{G}$ is the two-dimensional vector of the reciprocal lattice. In the limit $\gamma \to 0$ formula (4.13) reduces to

$$F = \frac{\pi}{M}\sum_{\mathbf{k}} k_x |f(\mathbf{k})|^2 \delta\left(\Omega_0^2(\mathbf{k}) - k_x^2 V^2\right). \tag{4.31}$$

As is seen from formula (4.31), equality $\Omega_0(\mathbf{k}) = k_x V$ determines the condition for phonon generation and cannot obviously be fulfilled at velocities lesser than the sound velocity. However, at $\gamma \neq 0$, the more general formula (4.30) gives a finite friction force, though its value must be small, being proportional to $\gamma V/\Omega_0^4(\mathbf{G})$ (at $V \to 0$). To obtain a realistic (for QCM experiments) estimate of the braking time of an adsorbed film forming a structure incommensurable with adsorbate, Sokoloff conceives of this structure as being partially disordered, that violates its translational symmetry and contributes significantly to friction, or uses the overestimated phonon damping time (10^{-3} s). In the latter case from formula (4.31) follows

$$F = -\frac{\pi^2 N}{G M V_s^2}\,|f(\mathbf{G})|^2\,,$$

where N is the number of atoms in the film, V_s is the sound velocity, and $\mathbf{G}$ is the minimum vector of the reciprocal lattice. In this case, as we have seen, the friction force does not depend on the velocity. Obviously, its value depends to a large degree on poorly known parameters N, V_s, $f(\mathbf{G})$, therefore, estimation of the role of this mechanism requires additional analysis. It is known, for example, that the phonon velocity in small-size films is closer to 100 m s^{-1} rather than to 1000 m s^{-1} (the value used in work [114]). On the other hand, the value of the Fourier-factor $f(\mathbf{G})$ must be essentially dependent on the distance z between the film and the surface, decreasing with increasing z.

Dynamic phonon friction, however, also arises in motion of individual atoms as well as AFM probes. Estimates of the corresponding forces may be made in the framework of the quantum perturbation theory [115]. In this case the processes of scattering of surface phonons are of primary importance. For the high-temperature acoustic spectrum of phonons corresponding to temperature T and condition $V/V_s \ll 1$, the friction force turns out to be

$$F \approx -\frac{S(k_B T)^2}{(\hbar V_s)^3}\left|U_{\mathbf{G}}(z)\right|^2 \frac{V}{V_s}\,, \tag{4.32}$$

where $U_{\mathbf{G}}(z)$ is the two-dimensional Fourier-factor of the atom-surface interaction potential, and S is the area of the unit cell. The z-dependence of the friction force is determined by the concrete form of the Fourier-factor $U_{\mathbf{G}}(z)$, and the quadratic temperature dependence is determined by the two-dimensional nature of the phonon spectrum of the surface.

Figure 20 illustrates the $\Delta t(z)$ dependence for braking a krypton atom on the silicon (111) surface [115] obtained on the basis of formula (4.32) at different temperatures. In calculations an interatomic potential of the form $V(r) = -C_6 r^{-6}\left[1 - 0.5(r_0/r)^6\right]$ with parameters $C_6 = 3.75 \times 10^{-78}$ J m^6, $r_0 = 0.38$ nm was used. Fig. 20 shows that the phonon mechanism may provide the braking time of 1ns observed in QCM experiments, if the atom is adsorbed at a realistic distance of 0.3 – 0.35 nN from the surface.

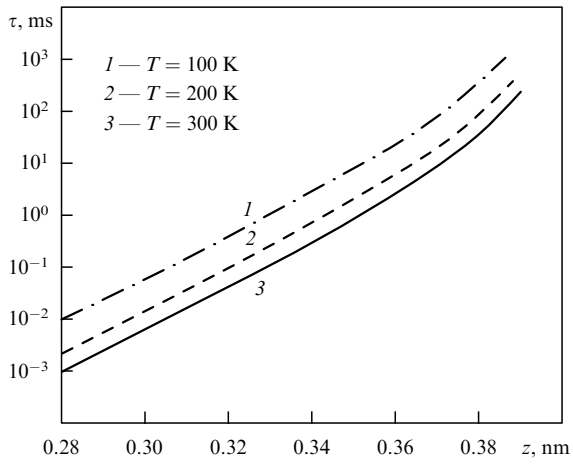

Figure 20. Theoretical dependence of the braking time for a krypton atom adsorbed on a Si(111) surface on the distance from the surface and the temperature. Phonon mechanism of friction. (From work [115].)

In work [75] the problem of phonon friction was considered in connection with braking an AFM probe. In the accepted model the presence of a vacuum interlayer (of atomic dimensions) between the probe and sample does not impede the passage of phonons transferring momentum and is taken into account through the change of the sound velocity. Then, in the Debye (low-temperature) approximation, the friction force acting on a probe with radius R is

$$F = -\frac{\pi^3}{45}\left(\frac{k_B T}{V_s \hbar}\right)^4 R^2 \hbar V \frac{V_t}{V_s}\,, \tag{4.33}$$

where V_t and V_s are the sound velocities for the tribocontact and in the volumes of bodies, respectively. At $R = 20$ nm, $V = 1$ m s^{-1}, $V_s = 6600$ m s^{-1} (silicon), $V_t/V_s \approx 0.1 - 0.01$, $T = 300$ K, the estimate of the friction force gives $F = 0.5 - 5$ pN. This value is comparable with values determined by other mechanisms of dynamic friction. Stoneham, however, called attention to the drawback of this

approach, in which contacting bodies are considered as phonon reservoirs [116].

4.6 Other theories

Closing the review of theoretical models, we will briefly touch on some other models of nanostructural friction.

Persson [117] studied the mechanism of lubrication friction for the purpose of interpreting experiments performed with the use of an SFA. It was assumed that tangential stress applied to the interface layer of molecules sandwiched between the plates of the SFA is a function of the slip velocity: $\sigma = \sigma(V)$. This relation was supported by numerical experiments. It was also postulated that the adsorbed film may be in the solid or liquid state, alternately 'oscillating' between these states during the motion of the upper plate in the stick – slip regime, and the thermodynamics of the corresponding phase transition are characterized by a phase diagram in the variables temperature – degree of coating.

If the film is in the liquid phase, the slip velocity of the upper plate of the SFA may be distinct from zero at arbitrarily small values of the shearing stress. If the film congeals, then $\sigma \neq 0$ and $V = 0$. Thus, the lack of sticking is connected with the formation of a two-dimensional liquid interlayer. This agrees with experiment. If the film is in the solid phase and has a structure commensurable with that of the substrate, this structure retains until σ reaches a critical value σ_0 at which the film transforms into the liquid phase. However, on decreasing σ down to values less than σ_0, friction remains low until the shearing stress reaches some new critical value at which the film congeals again. Thus, this model explains the hysteresis of friction forces observed in the SFA experiments.

Sokoloff [64] discussed the conditions of disappearance of friction in finite-size systems using a dynamic model of an isolated atomic chain. Since the phonon modes of a finite-size solid body are separated from each other by a relatively wide interval, it may occur that the distance between these modes exceeds a natural linewidth. In this case the transformation of a translational motion into vibration modes (and eventually into the thermal energy) is hampered and this motion may continue without losses for a long time. For a three-dimensional cubiform sample, in the acoustic limit the corresponding condition has the following form ($Na = L$ is the cube dimension, a is the lattice constant) [64]

$$\frac{(V_s\pi/Na)^2}{\omega} \gg \gamma .$$

Then at $V_s = 10^5$ m s^{-1}, $L = 1$ cm this condition gives $\gamma\omega \ll 10^{11}$ s^{-2} that can be valid for low-frequency acoustic modes.

Using the method of inelastic scattering of molecular helium beams, the authors of work [118] measured the oscillatory-motion damping constants (for motion along the normal to the surface) for molecules of typical lubricating materials (octane and hydrocarbons) on diamond (111), lead (111), ruthenium (001) and copper (111) substrates. In the far-infrared region (< 15 MeV), the measured damping constants were found to be 0.2 – 1.1 MeV. Hence, in this case we obtain an estimate $\omega\gamma = 10^{24} - 10^{25}$ s^{-2}. The half-width of absorption lines turned out to be in good agreement with the theoretical formula

$$\gamma = \frac{M\omega_0^2}{A\rho V_s} ,$$

where M is the mass of adsorbate, ω_0 is the oscillation frequency, A is the surface space occupied by adsorbate, ρ and V_s are the mass density of the substrate and the velocity of transverse phonons, respectively. The results of work [118] show that the damping of the translation motion of molecules in the direction of the surface normal are adequately explained by the phonon mechanism, if: first, the frequency of the oscillation of molecules is much less than the frequency of volume phonon modes; second, even weak chemical interactions capable of leading to the occurrence of a dominating contribution of electron excitations are absent.

Persson [119] proposed a new theory of the friction of rubber (polymer) on a solid surface. According to this theory the greatest contribution to the friction force is from internal friction determined by the fluctuation character of surface stresses acting on the rubber from the microridges of a solid surface.

Another contribution is connected with the adhesive force. At low slip velocities, the adhesive forces deform the surface of rubber in such a way that it fills the valleys of the surface relief. At very low velocities, the first mechanism is dominant, since most polymer materials exhibit considerable internal friction even at very low frequencies (of the order of 0.1 s^{-1}).

The main conclusions and problems of a theoretical nature to emerge from Section 4 can be summarized as follows:

On the whole, the level of theoretical understanding of friction mechanisms remains rather low because of a lack of a unified quantum theory taking into account all types of elementary processes occurring in the contact area. So far there is no universally accepted viewpoint regarding the quantitative characteristics and relative role of electron, electromagnetic and phonon excitation mechanisms, and a clear differentiation is lacking. At the same time it can be said with assurance that there are two types of nanostructural friction: static, independent of (or weakly dependent on) the velocity, and the dynamic, proportional to the velocity. The microscopic theory of static friction is so far phenomenological in character. Dynamic mechanisms have been studied in more detail, but also call for further examination.

Macroscopic contact mechanics provides an adequate interpretation of experimental 'friction-load' type dependencies and the results of measurements of the area of elastic nanocontacts, however, the simple extrapolation of the mechanical properties of materials to the nanostructural level may result in marked errors, since such parameters as the area of a contact, the shearing stress and the adhesion work may undergo considerable changes. Besides, contact models do not allow one to describe more complex effects associated with atomic and electron structures, chemical composition and microscopic mechanisms, and in the case of friction on the surfaces of alkaline-haloid crystals they are not effective at all.

The simple phenomenological (oscillator) model of the SS effect does not provide a deep insight into the nature of the periodicity of this process in actual experimental practice, when the contact area involves a large number of atoms. A fundamental weakness of this model is that it gives an incorrect dependence of the dissipative friction force on the contact stiffness.

The MD method, as applied to problems of nanoindentation and friction, on the whole gives a satisfactory description of the energetics, structure and dynamics of contacts as well as

a number of other tribological effects. However, there is a gap between the MD and actual experimental conditions, since in the MD simulation the experiments ultra-short time intervals, the high velocities of nano-probes and restricted statistics of particles are used. Increasing the simulation time (or the number of particles) up to realistic values is fundamentally impossible because of the enormous expenditure of computer time and accumulation of errors when calculating the kinetic energy of particles. This does not allow one to separate correctly the part of energy relating to dissipation. Therefore, the prediction of friction forces for actual experimental conditions when using AFMs still remains problematic. In this connection the development of quasistatic-type models based on the adhesive theory of bond breaking is a topical problem.

As to the dynamic mechanisms of friction, it should be noted that they all, despite existing distinctions, give (in the case of AFM) closely related values of friction forces of the order of 1 pN at probe velocities of about 1 m s^{-1}. In QCM and SFA experiments and in the modulation mode of AFMs, this mechanisms may play an important role, therefore, there is a need to perform detailed calculations of friction forces for concrete conditions. The presence of specific (for different mechanisms) dependencies of friction forces on the probe radius, temperature and other physical parameters of tribocontacts provides a possibility for a critical choice between available models by measuring numerical decrements in the vibration mode of an AFM as well as providing the basis for the development of new nondestructive methods for the diagnostics of nanostructural parameters. In the case of QCM experiments, the observed damping time may be determined by different effects, therefore, it is also necessary to compare theoretical end experimental data.

5. Technological applications

As is evident from the foregoing, the nanotribological aspects of the problem of contact interaction are connected with a broad spectrum of physical and chemical properties of surfaces and play a key role in many application areas, among which the following areas should be primarily noted: production and exploitation of magnetic recording devices; development of new surface coatings and modification of their tribological characteristics; nanolithography; mechanical engineering; chemical production; diagnostics of physical properties, composition, structure and relief of the surfaces of materials and so on.

In magnetic recording devices one of the most important problems is the fabrication and diagnostics of the properties of protective coatings with the aim of increasing their reliability and extending their life. Bhushan et al. [87] were the first to lay a foundation for application of AFMs for conducting technological and tribological tests of magnetic tapes, hard disks and different protective coatings. The authors of work [24] developed a depth-sensitive technique for multiple slip nanoindentation of surfaces making it possible to perform a quantitative comparison of the tribological characteristics of films deposited onto substrates of the same type. For the material interface in contact recording devices, surface degradation is the most serious problem. Triboelectromagnetism, causing the disruption of the molecular structures of lubricating coatings, is another severe problem. For these reasons in recent years in the magnetic industry preference has been given to disk sliders operating in the tapping mode [103] in which a stiff contact with a surface takes place only at the instants of the start and stop of slider motion. In prospect, however, the implementation of the contact mode will make it possible to increase considerably the writing density, the rate and quality of writing and reading.

Methods for combatting wear of the components of instruments and machines using the ion-plasma and ion-stimulated treatment of surfaces call for comprehensive information on wear mechanisms: abrasive wear, adhesion, material fatigue, erosion and fretting-corrosion. In practice, different combinations of these mechanisms, as a rule, are observed. For example, tribological problems relating to the wear of the components of mill machines used for crumbling plastic materials are concentrated around the processes of adhesive friction and degradation of surfaces, abrasive wear by the flow of crumbled materials, corrosion of instruments stimulated by gases and the products of plastic decomposition. The discussion of these and many other aspects of present-day industrial tribology can be found in work [120].

In the last decade considerable attention has been given to the probing modifications of surfaces as a method of nanolithography (see work [90] and the literature cited therein). Contact of the STM tip with the passivated surface of a silicon plate induces its oxidation, therefore, the process of fabrication of photomasks may be accomplished in the mode of contact interaction of the probe with the surface. There are several factors making this technology attractive: ultra-high resolution, the accuracy of accommodation and orientation of relief details as well as high throughput. However, in order that this technology becomes commercially profitable, the scan velocity in the 'scratch' mode must be raised up to 1 cm s^{-1}. In present-day commercial AFMs the velocities are three-four orders of magnitude lower. Hence, there is a need to investigate nanostructural friction over a wider interval of velocities.

Another technological line in nanolithography may open the way to noncontact ion modification of materials using nanobeams focused onto a surface by nanowires connected with the bracket of a scanning probing microscope [121].

Simulation of the dynamic characteristics of thin-film lubricating coatings occupies a highly important place in the solution of a rich variety of technological problems ranging from the problems of elastic hydrodynamical lubrication of toothed gearings and slip bearings to the tribology of the next generation of storage devices. Simulation allows one to reduce the existing gap between technical friction and nanotribiology and refines the theoretical understanding of the mechanisms of material degradation.

The possibilities of commercial use of nanostructural friction for activization of the process of tribochemical wear and the self-organization of molecular complexes on friction boundaries still call for further investigation.

At the present time there can be little doubt that the classical friction coefficient and the velocities of material wear on the nanostructural level are less than those on the macrolevel, whereas hardness, on the contrary, is higher. Hence, the operation of the future generation of micromachines may have peculiarities which cannot be predicted on the basis of simple similarity notions [4]. Nanotribological investigations with the use of AFMs do not allow one to predict uniquely the values of macroscopic friction and wear coefficients, since the direct proportionality between the friction force and the loading force results from overlapping

and interaction of the numerous microcontacts of surfaces, their elastic and plastic deformation, vibration smoothing and so on. Nevertheless, test investigations of the degradation and wear of surfaces because of friction conducted using the AFM method, which allows one to control the process of nanoindentation, have become an independent method for the engineering diagnostics of material surfaces and determination of a wide range of their physical and chemical properties.

6. Conclusions

The rich variety of experiments and theoretical models considered in the review demonstrates the considerable potential of nanoprobing microscopy and gives notions of the spectrum of available experimental and theoretical problems related to nanotribology. Progress in their solution and the practical implementation of the results of investigations will depend on the improvement of experimental equipment and the quality of new informations obtained in experiments, on the one hand, as well as on the efforts of theorists, on the other. Nevertheless, even today one can speak of the formation of a new promising line of surface physics – nanotribology. The most dramatic result of these investigations is the achieved possibility of measuring ultrasmall forces between a nanoprobe and surface atoms. The simplicity of the probing element itself is worthy of admiration: it is a mere sharp jut (hair) on the console, whose deformation is described in addition by one of the simplest physical models — the harmonic oscillator model! However, nanotribology cannot be considered a particular line of investigation associated only with the use of AFMs. In combination with nanoindentation — vertical probing, nanotribological investigations allow one to study the atomic structure of matter in three dimensions and not only to measure, but also to see it. This was undreamed of only a few years ago, and today this dream has been realized.

In conclusion I would like to express my gratitude to A M Stoneham for discussion of the aspects of the dynamic mechanism of friction and to K L Johnson, M Salmeron, H Holscher V V Pokropivny and B Bhushan for the preprints of their works and figures.

References

1. Binnig G, Quate C F, Gerber C *Phys. Rev. Lett.* **56** 930 (1986)
2. Mate C M et al. *Phys. Rev. Lett.* **59** 1942 (1987)
3. Carpick R E, Salmeron M *Chem. Rev.* **97** 1163 (1997)
4. Bhushan B, Israelachvili J N, Landman U *Nature* (London) **374** 607 (1995)
5. Krim J *Comments Condens. Matter. Phys.* **17** 263 (1995)
6. Stoneham A M, Ramos M A, Sutton P *Philos. Mag. A* **67** 797 (1993)
7. *Fundamentals of Friction: Macroscopic and Microscopic Processes* (Eds I L Singer, H M Pollock) (Dordrecht: Kluwer Acad. Publ., 1992)
8. *Physics of Sliding Friction* (Eds B N J Persson, E Tosatti) (Dordrecht: Kluwer, 1996)
9. Persson B N J *Sliding Friction: Physical Principles and Applications* (Berlin: Springer, 1998)
10. Sarid D *Scanning Force Microscopy* (New York: Oxford Univ. Press, 1991)
11. Hurtmann U *An Introduction to AFM and Related Methods* (TopoMetrix, 1997) p. 26
12. Bowden F P, Tabor D *The Friction and Lubrication of Solids* Parts 1 & 2 (Oxford: Clarendon Press, 1950 – 1964)
13. Marti A G, Hafner G, Spencer N D *Langmuir* **11** 4632 (1995)
14. Binggeli M, Christoph R, Hintermann H E *Tribol. Lett.* **1** 13 (1995)
15. Nakayama K, Bou-Said B, Ikeda H *Trans. ASME J. Tribol.* **119** 764 (1997)
16. Hu J et al. *Surf. Sci.* **327** 358 (1995)
17. Schumacher A et al. *J. Vac. Sci. Technol. B* **14** 1264 (1996)
18. Dayo A, Alnasrallah W, Krim J *Phys. Rev. Lett.* **80** 1690 (1998)
19. Tabor D, Winterton R *Proc. R. Soc. London Ser. A* **312** 435 (1969)
20. Israelachvili J N, Tabor D *Nature* (London) **241** 148 (1973)
21. Watts E T, Krim J, Widom A *Phys. Rev. B* **41** 3466 (1990)
22. Krim J, Solina D H, Chiarello R *Phys. Rev. Lett.* **66** 181 (1991)
23. Daly C, Krim J *Phys. Rev. Lett.* **76** 803 (1996)
24. Deng H, Barnard J A *IEEE Trans. Mag.* **33** 3151 (1997)
25. Binnig G,Rohrer H *Sci. Am.* (9) 50 (1982); Binnig G, Rohrer H *Usp. Fiz. Nauk* **154** 261 (1988)
26. Israelachvili J N *Intermolecular and Surface Forces* (London: Acad. Press, 1992)
27. Deryagin B V, Churaev N V, Muller V M *Poverkhnostnye Sily* (Surface Forces) (Moscow: Nauka, 1985) [Translated into English (New York: Consultants Bureau, 1987)]
28. Teibor D *Trenie i Iznos* **15** 296 (1994)
29. Edel'man V S *Prib. Tekh. Eksp.* (5) 25 (1989); *Prib. Tekh. Eksp.* (1) 24 (1991)
30. Suslov A A, Chizhik S A *Materialy, Tekhnologii, Instrumenty* **2** 78 (1997)
31. Linnemann R et al. *J. Vac. Sci. Technol. B* **14** 856 (1996)
32. Ogletree D F, Carpick R W, Salmeron M *Rev. Sci. Instrum.* **67** 3298 (1996)
33. Radmacher M et al. *Proc. SPIE* **2384** 141 (1995)
34. Sader J E *Rev. Sci. Instrum.* **66** 4583 (1995)
35. Lanz M A et al. *Phys. Rev. B* **55** 10776 (1997)
36. Bar G, Brandsch R, Whangbo M-H *Surf. Sci.* **411** L802 (1998); Wang L *Surf. Sci.* **429** 178 (1999)
37. Holscher H, Schwarz U D, Wiesendanger R *Appl. Surf. Sci.* **140** 344 (1999)
38. Giessibl F J et al. *Appl. Surf. Sci.* **140** 352 (1999)
39. Carpick R W, Dai Q, Ogletree D F, Salmeron M *Tribol. Lett.* **5** 91 (1998)
40. Morita S, Fujisava S, Sugawara Y *Surf. Sci. Rep.* **23** 3 (1996); *Phys. Rev. B* **57** 3785 (1998)
41. Hu J et al. *Surf. Sci.* **327** 358 (1995)
42. Carpick R W et al. *J. Vac. Sci. Technol. B* **14** 1289 (1996)
43. Carpick R W, Agrait N, Ogletree D F, Salmeron M *Langmuir* **12** 3334 (1996)
44. Cleveland J P, Radmacher M, Hansma P K, in *Forces in Scanning Probe Methods* (Eds H-J Gunterodt et al.) (Dordrecht: Kluwer, 1995) p. 543
45. Yamanaka K, Ogiso H, Kolosov O *Appl. Phys. Lett.* **64** 178 (1994)
46. Oliver W C, Pharr G M *J. Mater. Res.* **7** 1564 (1992)
47. Carpick R W, Ogletree D F, Salmeron M *Appl. Phys. Lett.* **70** 1548 (1997); Lantz M A et al. *Appl. Phys. Lett.* **70** 970 (1997)
48. Kerssemakers J, De Hosson J Th M *Appl. Phys. Lett.* **67** 347 (1995); *Appl. Phys.* **80** 623 (1996); *J. Appl. Phys.* **81** 3763 (1997); *Surf. Sci.* **417** 281 (1998)
49. Moiseev Yu N, Mostepanenko V M, Panov V I *Phys. Lett. A* **132** 354 (1988); Johansson P, Apell P *Phys. Rev. B* **56** 4159 (1997)
50. Dedkov G V, Rekhviashvili S Sh *Pis'ma Zh. Tekh. Fiz.* **23** 88 (1997) [*Tech. Phys. Lett.* **23** 452 (1997)]; **25** 61 (1999) [**25** 67 (1999)]
51. Kelly K F et al. *J. Vac. Sci. Technol. B* **14** 593 (1996); *Science* **273** 1371 (1996)
52. Dai H et al. *Nature* (London) **384** 147 (1996)
53. Dedkov G V *Pis'ma Zh. Tekh. Fiz.* **23** 31 (1997) [*Tech. Phys. Lett.* **23** 469 (1997)]; *Pis'ma Zh. Tekh. Fiz.* **69** 128 (1999)
54. Frantz P, Agrait N, Salmeron M *Langmuir* **12** 3289 (1996)
55. Klein J, Kumacheva E *Science* **269** 816 (1995)
56. Zworner O, Holscher H, Schwarz U D, Wiesendanger R *Appl. Phys. A* **66** S263 (1998)
57. Holscher H et al. *Phys. Rev. B* **57** 2477 (1998)
58. Allers W et al. *Appl. Surface Sci.* **140** 247 (1999)
59. Fujisawa S et al. *Jpn. J. Appl. Phys.* **33** 3752 (1994); *Phys. Rev. B* **51** 7859 (1995); *Tribol. Lett.* **1** 121 (1996)
60. Yoshisawa H, Chen Y-L, Israelachvili J N *Wear* **168** 161 (1993)
61. Tomlinson I *Philos. Mag.* **7** 905 (1929)

62. McClelland G M, Glosli J N, in *Fundamentals of Friction: Macroscopic and Microscopic Processes* (Eds I L Singer, H M Pollock) (Dordrecht: Kluwer, 1992) p. 405
63. Gyalog T, Thomas H *Europhys. Lett.* **37** 195 (1997)
64. Sokoloff J B *Phys. Rev. Lett.* **71** 3450 (1993)
65. Johnson K L, Woodhouse J *Trib. Lett.* **5** 155 (1998)
66. Dedkov G V, Dyshekov M B *Zh. Tekh. Fiz.* **70** (7) 96 (2000) [*Tech. Phys.* **45** 909 (2000)]; Dedkov G V, Dyshekov M B *Surf. Sci.* (1999, submitted)
67. Landman U, Luedtke W D, in *Scanning Tunneling Microscopy III: Theory of STM and Related Scanning Probe Methods* (Eds R Wiesendanger, H-J Güntherodt) (Berlin: Springer-Verlag, 1993) p. 207
68. Sorensen M R, Jacobsen K W, Stolze P *Phys. Rev. B* **53** 2101 (1996)
69. Buldum A, Ciraci S *Phys. Rev. B* **57** 2468 (1998)
70. Durig U, in *Physics of Sliding Friction* (NATO ASI Series, Ser. E, Vol. 311, Eds B N J Persson, E Tosatti) (Dordrecht: Kluwer Acad. Publ., 1996) p. 299
71. Fujisawa S, Sugarawa Y, Morita S *Philos. Mag. A* **74** 1329 (1996)
72. Enachescu M, Van den Oetelaar R J A, Carpick R W, Ogletree D F, Flipse C F J, Salmeron M *Phys. Rev. Lett.* **81** 1877 (1998)
73. Johnson K L *Contact Mechanics* (Cambridge: Cambridge Univ. Press, 1985 – 1987) [Translated into Russian (Moscow: Mir, 1989)]
74. Israelachvili J N, in *Fundamentals of Friction: Macroscopic and Microscopic Processes* (Eds I L Singer, H M Pollock) (Dordrecht: Kluwer, 1992) p. 351
75. Dedkov G V *Mater. Lett.* **38** 360 (1999); *Wear* **232** 145 (1999)
76. O'Shea S J, Welland M E, Pethica J B *Chem. Phys. Lett.* **223** 336 (1994)
77. Luedtke W D, Landman U *Comp. Mater. Sci.* **1** 1 (1992)
78. Green J-B D, McDermott M T, Porter M D *J. Phys. Chem.* **99** 10960 (1995)
79. Cleveland J P, Schaffer T E, Hansma P K *Phys. Rev. B* **52** R8692 (1995)
80. Landman U et al., in *Computations for the Nano-Scale* (NATO ASI Series, Ser. E, Vol. 240, Eds P E Blöchl, C Joachim, A J Fisher) (Dordrecht: Kluwer, 1993)
81. Sorensen M R, Jacobsen K W, Stolze P *Phys. Rev. B* **53** 2101 (1996)
82. Pokropivny V V, Skorohod V V, Pokropivny A V *Trenie i Iznos* **17** 579 (1996); Pokropivny V V, Skorohod V V, Pokropivny A V *Modelling Simul. Mater. Sci. Eng.* **5** 579 (1997); *Materials Lett.* **349** (1997)
83. Perez R, Payne M C *Phys. Rev. Lett.* **75** 4748 (1995)
84. Nelson J S, Dodson B W, Taylor R A *Phys. Rev. B* **45** 4439 (1992)
85. Sutton A P, Todorov T N *J. Phys. Chem. Solids* **55** 1169 (1994)
86. Heinicke G *Tribochemistry* (Berlin: Akademie-Verlag, 1984) [Translated into Russian (Moscow: Mir, 1987)]
87. Bhushan B, in *Handbook of Micro/Nanotribology* Ch. 1 (Ed. B Bhushan) (Boca Raton: CRC Press, 1995)
88. Schwarz U D et al. *Phys. Rev. B* **56** 6997 (1997); Xin-Chun Lu, in *11-th Jufer. Conf. on Surface Modification of Methods by Jon Beams* (*Beijing, 1999*) p. 135; *Surf. Coat. Technol.* (2000, in press)
89. Nakahara S, Langford S C, Dickinson J T *Tribol. Lett.* **1** 277 (1995)
90. Quate C F *Science* **386** 259 (1997)
91. Bhushan B, in *Proc. IEEE. 9th Annu. Inter. Workshop on Micro-Electro Mechanical Systems* (New York: IEEE, 1996)
92. Bhushan B, Koinkar V N *Appl. Phys. Lett* **64** 1653 (1994)
93. Schluger A L et al. *Phys. Rev. B* **52** 11398 (1995)
94. Sutton A P, Todorov T N *J. Phys. Chem. Solids* **55** 1169 (1994)
95. Landman U, Luedtke W D *Wear* **153** 3 (1992)
96. Abraham F F, Rutge W E, Alexopoulos P S *Comput. Mater. Sci.* **3** 21 (1994)
97. Overney R M, Leta D P *Tribol. Lett.* **1** 247 (1995)
98. Krim J, Chiarello R J *J. Vac. Sci. Technol. A* **9** 2566 (1991)
99. Tamura H et al. *Appl. Surf. Sci.* **119** 335 (1997)
100. Depondt Ph, Ghazali A, Levy J-C S *Surf. Sci.* **419** 29 (1998)
101. Rubio G, Agrait N, Vieira S *Phys. Rev. Lett.* **76** 2602 (1996)
102. Persson B N J,Tosatti E *Surf. Sci.* **411** L855 (1998)
103. Talke F E, in *Proc. 8th Inter. Conf. on Tribology* (Eds S S Eskildsen et al.) (Aarhus: DTI Trib. Centre, 1998) p. 585
104. Maugis D J *J. Colloid. Interface Sci.* **150** 243 (1992)
105. Barthel E *J. Colloid. Interface Sci.* **200** 7 (1998); *Thin Solid Films* **330** 27 (1998)
106. Holscher H, Schwarz U D, Wiesendanger R *Europhys. Lett.* **36** 19 (1996); *Surf. Sci.* **375** 395 (1997)
107. Tomassone M S, Widom A *Phys. Rev. B* **56** 4938 (1997)
108. Dedkov G V, Kyasov A A *Pis'ma Zh. Tekh. Fiz.* **25** 360 (1999) [*Tech. Phys. Lett.* **25** 466 (1999)]
109. Dedkov G V, Kyasov A A *Phys. Lett. A* **259** 38 (1999)
110. Dedkov G V, Kyasov A A *Surf. Sci.* (1999, in press)
111. Pendry J B *J. Phys. C* **9** 10301 (1997)
112. Volokitin A I, Persson B N J *J. Phys. C* **11** 345 (1999)
113. Sokoloff J B *Phys. Rev. B* **52** 5318 (1995)
114. Sokoloff J B *Phys. Rev. B* **51** 15573 (1995)
115. Dedkov G V *Phys. Stat. Solidi. A* **179** (1) (2000)
116. Stoneham M A (1999, private communication)
117. Persson B N J *Phys. Rev. B* **50** 4771 (1994)
118. Fuhrmann D, Woll Nh *New J. Phys.* **1** 1.1 (1998)
119. Persson B N J *Surf. Sci.* **401** 445 (1998)
120. *Proc. 8th Inter. Conf. on Tribology* Vol. 1, 2 (Eds S S Eskildsen et al.) (Aarhus: DTI Trib. Centre, 1998)
121. Dedkov G V *Nucl. Instrum. Methods B* **143** 584 (1998)